OET | Opto-Electronic Technology

30 years of nanoimprint: development, momentum and prospects

Wei-Kuan Lin, L. Jay Guo*

https://doi.org/10.29026/oet.2025.250001

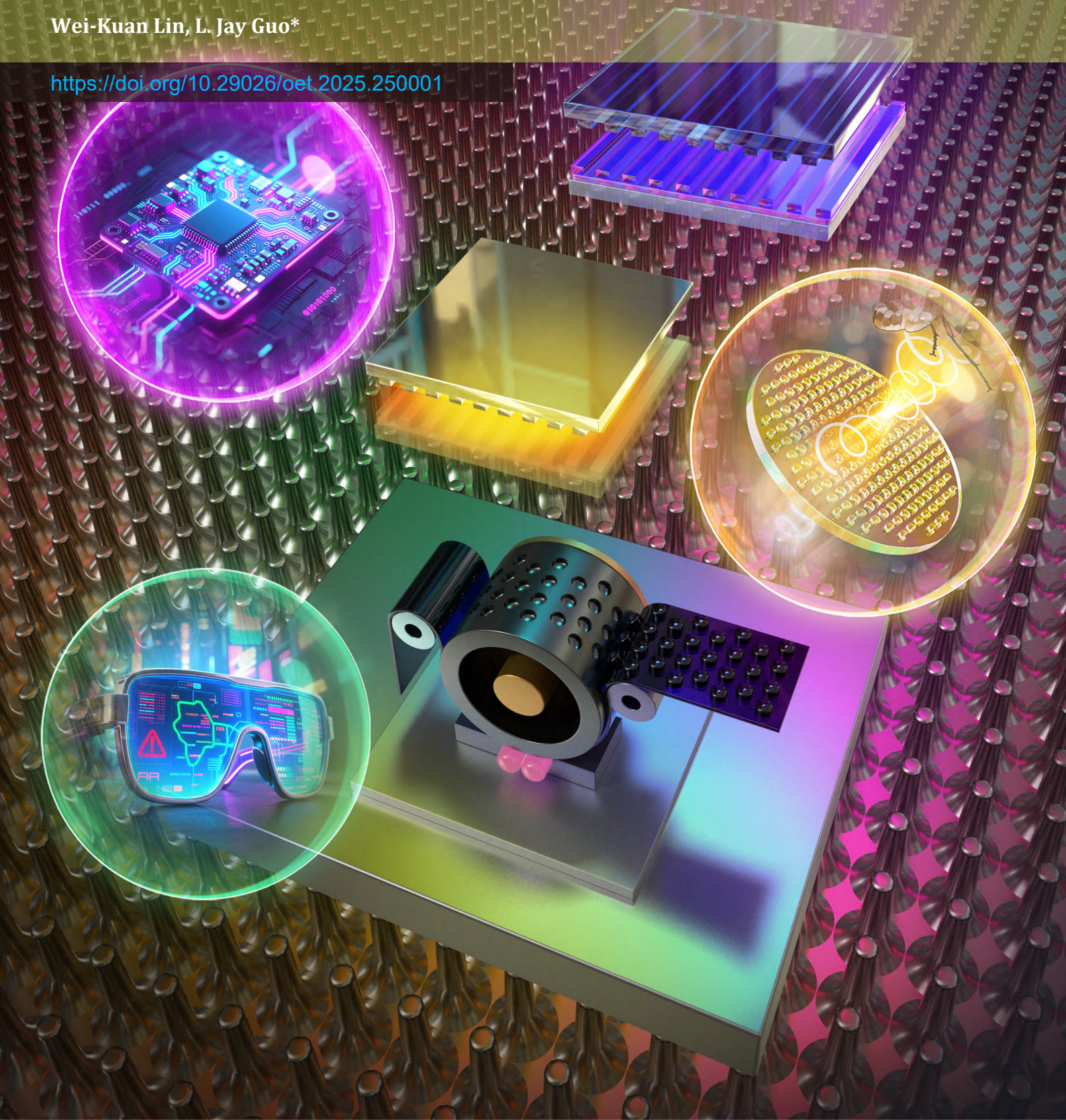

OET | Opto-Electronic Technology

CN 51-1811/O4 ISSN (Print) 2097-6003

30 years of nanoimprint: development, momentum and prospects

Wei-Kuan Lin and L. Jay Guo

Citation: Lin W-K, Guo LJ. 30 years of nanoimprint: development, momentum and prospects. *Opto-Electronic Technology* **1**, 250001(2025).

https://doi.org/10.29026/oet.2025.250001

Received: 12 May 2025; Accepted: 23 June 2025; Published online: 29 June 2025

OET | Opto-Electronic Technology
www.oejournal.org/oet

Review
July 2025, Vol. 1, No. 1

DOI: 10.29026/oet.2025.250001 | CSTR: 32419.14.oet.2025.250001

Open Access

30 years of nanoimprint: development, momentum and prospects

Wei-Kuan Lin and L. Jay Guo*

Abstract: 2025 marks the 30th anniversary of nanoimprint lithography (NIL). Since its inception in 1995, and through global efforts over the past three decades, nanoimprint has emerged as the primary alternative to extreme ultraviolet (EUV) lithography for deep-nanoscale silicon (Si) electronics. Numerous semiconductor companies have recognized NIL's manufacturing quality and are actively being evaluated for the production of the most advanced semiconductor devices. Nanoimprinting's potential extends beyond silicon chip fabrication and wafer-scale applications. With its high throughput and 3D patterning capabilities, NIL is becoming a key technology for fabricating emerging devices, such as flat optics and augmented reality glasses. This review summarizes the key developments and applications of nanoimprint lithography, with a particular focus on the latest industry advancements in nano-Si device manufacturing and nanophotonics applications.

Keywords: nanoimprinting; manufacturing; high-volume production; semiconductor

Introduction

Nanoimprint lithography (NIL) was first introduced by Chou et al.[1,2] to provide a cost-effective solution for high-resolution nanopatterning across a wide range of applications, such as fabricating nanoscale single-domain magnets[3]. In his seminal work[1,2], Chou employed a patterned hard mold with 25 nm feature size to mechanically press onto a substrate coated with a thin PMMA layer at elevated temperatures. This process demonstrated, for the first time, that mechanical molding could reliably produce features at the nanometer scale, orders of magnitude smaller than what was previously considered possible in plastic molding. This breakthrough fundamentally challenged the prevailing assumptions about the limitations of mechanical patterning. Another critical finding from this early work was that the mold protrusions could nearly displace all the polymer resist, leading to a near-zero residual layer thickness. This phenomenon is essential for achieving high-resolution nanostructures.

Following these foundational advances, Chou's group conducted a comprehensive series of studies that laid the groundwork for the development and industrialization of NIL. Key contributions included: demonstrating sub-10 nm imprinting resolution for metal contact structures[4,5], identifying key process parameters, particularly the mold–resist interface[4,6], characterizing mold durability and pattern fidelity for large-scale production[7], exploring NIL's unique features, such as imprinting on non-planar surfaces, direct 3D patterning[8], and multilayer structuring[9], developing new NIL systems, such as roller-based imprinters[10], and establishing the first NIL-focused commercial enterprise. Chou's team also demonstrated a broad range of NIL applications, including high-storage disks[3,11,12], the first silicon nanoelectronic devices[13], sub-wavelength optical components[14], organic thin-film transistors[15], and nanofluidic devices[16], showcasing NIL's versatility and transformative potential.

Later, Haisma et al.[17] (mold lithography) and Colburn et al.[18] (step and flash imprinting) developed UV nanoimprinting lithography, respectively, by using slightly different implementation methods and addressing the high-temperature requirements of thermal imprinting. In 1998, the roller-based NIL was proposed to reduce the required force and achieve uniform imprinting[10]. The work inspired the later development of high-throughput yet low-cost solutions for continuous nanopatterning[10,19]. In 1999 and 2000, Lebib et al. and Heidari et al. demonstrated the larger-scale patterning capability at the 4-inch and 6-inch wafer-level with sub-100 nm resolution respectively[20,21]. In 2003, nanoimprinting technology was first selected for International Technology Roadmap for Semiconductors (ITRS) for patterning 32-nm and beyond technology nodes[22]. In 2004,

Received: 12 May 2025
Accepted: 23 June 2025
Published online: 29 June 2025

Department of Electrical Engineering and Computer Science, University of Michigan, Ann Arbor 48109 , USA.
*Correspondence: LJ Guo, E-mail: guo@umich.edu

Molecular Imprint Inc. launched the first step-and-repeat nanoimprinting tools that patterned an entire wafer by using a small stamp on a field-to-field basis[23]. This idea was then used to make and replicate a large working template to decrease the cost of molds[8]. The composite mold strategy was also developed in the 2000s. It incorporates a rigid patterned layer supported by a flexible or soft intermediate layer and a backing substrate to ensure conformal contact over the entire imprinting area[24,25]. With this design, low defect rates and high-fidelity imprinting with sub-50 nm resolution can be simultaneously achieved. As a result, the composite mold approach has been widely adopted for imprinting processes that target moderate resolution and high quality[24]. In 2023, Canon launched the first-ever semiconductor-grade nanoimprinting tools that match the industry's demanding requirements, advancing nanoimprinting lithography to a new era.

As the NIL technology matures, several applications have been demonstrated. Some hard disk companies have applied the concept of NIL to develop patterned magnetic nanostructures to expand the disk density beyond 1 Tb/in^2 by creating magnetic nanostructures with small feature sizes (<20 nm) and tight pitch spacings (< 30 nm)[26,27]. High-resolution polymer OLED was fabricated by using NIL in 2002[28]. Since 2010, NIL has also been used to manufacture wafer-level micro-optics to fabricate compact optical modules for mobile device applications at a high volume. The high throughput and large-scale features are also used for display or panel-sized nanopatterning applications. It is also widely used in research for microfluidic devices and biomedical applications. As new applications, such as next-generation gene sequencing, augmented reality, flat-optics, semiconductor devices, and several others emerged after 2020, NIL has finally found its niche. These new applications require the technology to be high-resolution, large-area, and have tight process control, which perfectly caters to NIL's advantage, making NIL irreplaceable. It is expected that these applications will maintain a high growth rate in the following years and can finally benefit from the developments of NIL.

In this review, we will first introduce the essential elements of nanoimprinting lithography and identify the key innovations of NIL over the past 30 years. We will discuss the long-standing issues of nanoimprinting and the general solutions for the challenges. In the 2nd part of the manuscript, we will focus on the current application of NIL in industrial manufacturing. Examples and manufacturing standards will be present. The last part will discuss the current trends and direction in the academic research area. This work serves as a review of the technological advancements in NIL, with a focus on the more recent developments, especially those from the industry. These represent the views of the authors, who do not intend to report the history of NIL. The readers are referred to many outstanding reviews published previously.

The basic types of NIL

Thermal nanoimprinting (T-NIL)

Thermal nanoimprinting is the first kind of nanoimprinting lithography[1]. The working principle of thermal imprinting is shown in Fig. 1(a). It starts with patterning a mold with the inverse tone of the final structure. Many types of thermoplastic materials, such as polystyrene, PMMA, and polycarbonate, can be used as NIL resist. After the resist is spin-coated onto a substrate, the mold is then pressed into the resist material at 50–80 °C above the resist's glass transition temperature (T_g) for a few minutes to allow the highly viscous polymer to flow and fill the voids between the mold and the substrate. Then, the substrate is cooled and separated from the master mold[29].

Theoretically, as long as the materials can be heated up to a glassy state with sufficient mobility under a reasonable temperature and pressure, materials can be patterned using thermal nanoimprinting lithography. The direct benefit is that nanostructures can be patterned on widely accessible materials at a meager cost, allowing users to achieve versatile functionalities by incorporating different functional materials into the nanostructures. It also allows direct molding of integrated photonic devices in a single step, e.g., imprinted polymer microring resonators[30–34]. Thermal nanoimprinting can also be used to pattern sheets of materials directly, such as thermoplastic and nanocellulose films, without coating an additional layer of imprinting resist.

Even though the thermoplastic becomes flowable under high temperatures and pressure in T-NIL, the polymer's viscosity usually remains high, resulting in a prolonged imprinting time. Additionally, these thermoplastic resists tend to stick to the mold, which seriously affects the fidelity and quality of the pattern definition. Surfactants for easy mold releasing can be incorporated into resist formulation.

UV nanoimprinting

Soon after the first demonstration of thermal NIL, the ultraviolet NIL (UV-NIL) process was developed by using photo-curable resin instead of thermoplastic materials to avoid high-temperature heating procedures[18]. The overall process procedure is illustrated in Fig. 1(b). UV-nanoimprinting starts by coating/dropping UV-curable precursor resins on the substrate and then pressing the mold with pressure. Since the UV resin is intrinsically fluid-like, the imprinting can be carried out at ambient temperature, thus improving process throughput. After applying pressure with sufficient time to force the resist flow into the voids on the mold, UV light triggers the cross-linking of the UV resist to form a stable nanostructure. Finally, the mold and the imprinted substrate are separated. The low imprinting temperature property also allows UV-NIL to be implemented on other substrates, such as plastic films. However, UV shrinkage of the resins is one of the concerns that can cause pattern distortion and demolding difficulties.

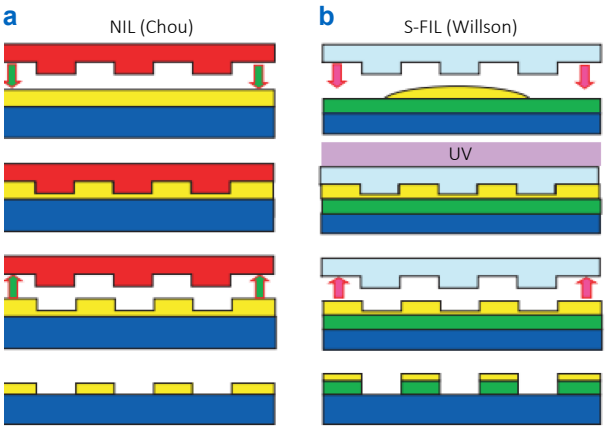

Fig. 1 | Basic imprinting type of nanoimprinting lithography. (**a**) Thermal NIL developed by Chou. (**b**) UV-imprinting/step-flash imprinting developed by Willson. Figure reproduced with permission from ref.[35], IOP Publishing.

NIL mold

NIL produces a replica of the imprinting mold, including the edge roughness of the patterns on the mold[36]. Therefore, the master mold must be fabricated with high-resolution technology to ensure its quality. The roughness of the etched pattern surface can potentially cause an increase of frictional force between the mold and resist, leading to pattern breakage during the demolding process. In general, the intense inductively coupled plasma (ICP) power and the Bosch process with scallop structures can significantly cause roughness and should be avoided.

When designing the mold patterns, the layout effect needs to be considered. Even though nanoimprinting lithography is not limited by optical diffraction, the final imprinting quality can still be affected by the pattern layout. Loading effect or high aspect ratio structures can result in non-uniform resist issues and void defects[37]. Several technologies, such as inkjet dispensing, have been dedicated to solving these issues[38]. Having a low surface energy of the mold is also crucial to the pattern fidelity during demolding. The resist can stick to the mold and cause permanent defect issues. Surface energy reduction can be achieved by coating a fluorosilane-based self-assembled monolayer with solvent or vapor incubation[39].

NIL by hard mold

The mold of NIL can be generally categorized into two major types based on mold stiffness: the hard mold and the soft mold, suited for different applications[40–42]. The hard mold materials are typically silicon, dielectric materials, and metals with high Young's modulus[43]. The hard mold's high toughness and high strength prevent the mold from deformation during the high-pressure imprinting process. Most high-resolution applications, such as semiconductor device imprinting, use this method to achieve higher pattern fidelity[44–47]. Figure 2(a) shows that sub-10 nm contact holes are faithfully imprinted using hard mold NIL and form an Au contact after metal evaporation and the resist liftoff process[5].

On the other hand, hard mold imprinting can pose challenging issues. First, non-uniform pressure can arise from the thickness variation of the substrate/mold, causing imprinting defects or even mold/wafer breakage. The use of pressurized air to imprint is of particular significance in ensuring uniform pressure in a situation like this[47]. Second, providing the conformal contact between mold and substrate is difficult. The presence of particles, non-flat or non-parallel surfaces, or even air trapped between the supporting plate can lead to non-conformal contact, resulting in imprinting defects[47].

NIL by composite mold

Soft NIL has been developed to circumvent the disadvantages of hard mold NIL with slightly compromised pattern fidelity. The soft nanoimprinting utilized high-flexibility materials, such as polydimethylsiloxane (PDMS)[48,49] and perfluoro-polyethers (PFPE)[50,51], as the imprinting mold. The high flexibility and low surface energy feature allow the mold to deform slightly with the presence of particles or residual contaminants, providing better contact between the mold and the substrate. Due to the benefits, the soft-NIL can be easily implemented under less restricted conditions. It has a higher dust tolerance than hard mold NIL. Moreover, soft NIL can be incorporated into the roller-based imprinting system for high throughput applications due to its flexible features[52]. Another essential feature of soft NIL is that it can be applied to a curved surface to expand its applicability, which is impossible by traditional NIL or challenging to achieve by photolithography[53].

One significant challenge of using soft molds for patterning is mold distortion during the imprinting process, limiting the achievable resolution, aspect ratio, and pattern density[36]. This issue can be lessened using a composite mold strategy[54], where thin high-modulus materials (such as polyurethane acrylate resin[54] or high-modulus PDMS[55]) with surface relief structures grafted on top of the low-modulus materials and flexible carriers, such as regular PDMS, thin glasses, or PET films. This strategy combines the advantages of the high-resolution property of the rigid mold NIL, derived from the high-toughness patterned layer, with the conformal feature of the soft and flexible stamp substrate. As shown in Fig. 2(b), a composite mold consisting of rigid features on a flexible PDMS support can successfully achieve sub-15 nm resolution on a flat substrate and faithfully duplicate gratings structure with 200 nm pitch on a cylindrical surface of a single mode optical fiber with a 125 μm diameter[25,54]. Another implementation of composite mold is the so-called substrate conformal imprinting lithography (SCIL), where a deformable cushion layer is formed between the rigid nanopatterned layer and the stiff support plate, providing out-of-plane flexibility,

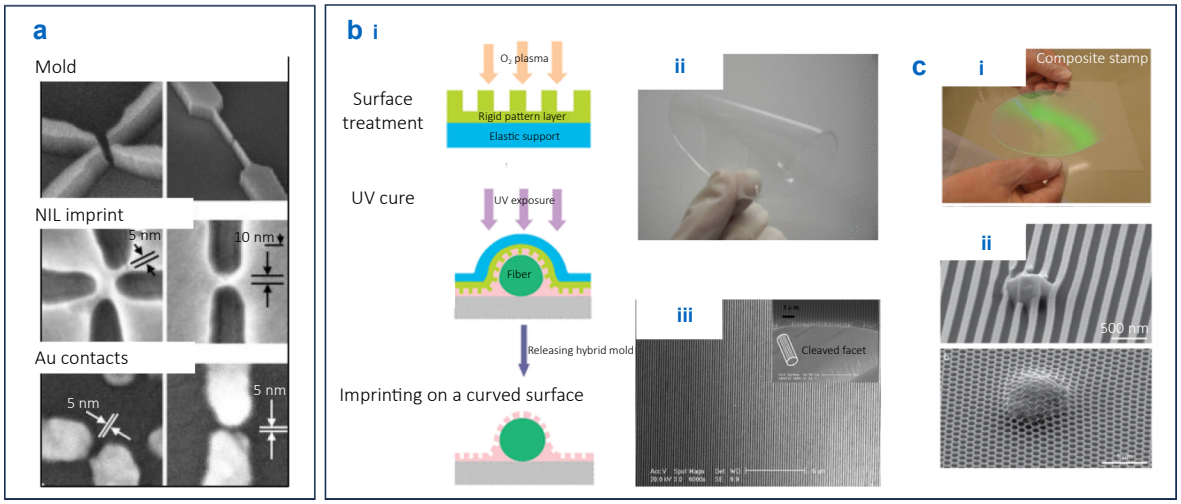

Fig. 2 | Different types of molds in NIL. (**a**) Hard mold is used for high-resolution patterning. (**b**) Flexible composite mold can be used for imprinting on a curved surface. (**b-i**) The imprinting process. (**b-ii**) The flexible composite mold. (**b-iii**) The imprinted grating structures on the optical fiber. (**c**) The substrate conformal nanoimprinting lithography can provide high-resolution conformal imprinting by using the composite mold. (**c-i**) The composite mold. (**c-ii**) The conformal imprinting over particle contaminants. Figure reproduced with permission from: (a) ref.[5], AIP Publishing; (b) ref.[25], American Chemical Society; (c) ref.[24], under a Creative Commons Attribution License.

while retaining in-plane stiffness to preserve pattern fidelity and alignment precision. Figure 2(c) demonstrates that high-quality, high-resolution patterning can still be achieved despite dust particles by using this SCIL. The composite mold strategy is widely used for high throughput and large-scale applications, such as wafer-level imprinting and roller-based imprinting. The composite mold strategy has become one standard solution for modern nanoimprinting technology.

Working stamp

The primary concern in NIL is the high cost of the imprinting mold and its limited lifetime. Fabricating an enormous mold with a 300 mm wafer size through electron beam (E-beam) writing is costly and impractical. In addition, because the molds directly interact with the resist and the substrates, they are susceptible to damage. As the most expensive element in the NIL system, the short life span of the mold can significantly increase the cost of ownership and potentially raise quality concerns about the process.

To address the issues, the working stamp strategy is developed, in which a working stamp is duplicated from the master mold and is used to perform the actual imprinting[56,57]. Using a cm-sized master mold prepared by E-beam writing and performing the step-and-repeat imprinting on a large substrate, a large working stamp with wafer-scale or even larger size with panel size can be replicated.

The working stamp method can also increase the lifetime of the master mold to reduce the cost further. In most cases, the master mold can only perform several hundred times of imprinting before considerable degradation. However, by using the working templates, the lifetime of the master mold can be extended by several orders. As an example, in semiconductor manufacturing, the E-beam master mold can make >100 replicas, and each replica can pattern >1000 wafers, leading to an equivalent master template life of >100,000 wafers, close to the lifetime of the reticles in traditional photolithography[44]. In metalens applications, the use of a working stamp also extended the lifetime of the master mold by 15–20×, allowing the fabrication of >10,000 replicated wafers by using one master mold[58]. The working stamp idea is now widely adopted in academics and industry, even for the most advanced processes. Various working stamps have been developed, such as soft-working stamps[58], hard-working stamps[44], large-size working stamps, and water-soluble working stamps[59] for different applications. Dedicated tools have been produced for working mold replications[60,61].

Recent advancements in NIL molds

In addition to the molds mentioned above, several other types of molds—such as super-resolution imprinting molds, high-durability working stamps, and natural molds —are also being actively developed. Typically, the feature sizes on these molds must match the desired pattern dimensions, making the fabrication of molds with ultra-fine structures particularly challenging. However, it has been shown that special treatments, such as heat treatment[62] or mechanical pressing[63], can effectively reduce the feature sizes on imprinting molds, enabling the generation of even smaller structures[64]. For example, Pina-Hernandez demonstrated in reference[62] that the imprinting feature size could be reduced from 55 nm to 10 nm after two shrinking cycles by using silsesquioxane imprint resist material[65].

Most of the aforementioned working stamps are made from polymer materials. While they offer high flexibility,

their low melting point and low modulus limit their suitability for T-NIL and lead to durability issues. To overcome this limitation, durable crystalline working templates have been developed by imprinting UV-curable resin mixed with nanoparticles —such as ZrO_2 and TiO_2 —followed by annealing[66,67]. These hard molds exhibit high pattern fidelity over more than 100,000 molding cycles without delamination or breakage.

Besides artificially making the imprinting templates, the molds can also made from natural nanostructures, such as cicada wings[68] and collagen fibers[69], to fabricate biomimetic structures at low cost. These biomimetic patterns have proven effective in preventing bacterial adhesion, enhancing cell coupling, and supporting tissue engineering applications.

NIL resist

Nanoimprinting resist is another critical element of NIL that directly interacts with the mold and is patterned in nanoscales. Depending on the functionality, the imprinting resist can be used as a reactive ion etching (RIE) mask to transfer the pattern to the underlying layer (NIL + RIE method) or directly used as the functional structures for the products (direct NIL method), such as polymer microlens and grating, as shown in Fig. 3(a)[70,71]. Excellent etching properties are desired to achieve better pattern transfer when used as an etching mask. The residual layer thickness control and the ashing completeness can also be critical. When used directly as part of the final device, the properties of the imprinting resist, including refractive index, conductivity, and optical transparency, will directly influence the functionality of the final structure.

To achieve high-quality imprinting, several factors need to be considered[72]. First, the NIL resist should be highly deformable under applied pressure and have sufficient mechanical strength and good mold-releasing properties. Second, the adhesive force between the resist and the substrate must be greater than the frictional force between the resist and the mold. In this regard, adhesive promotion coating is sometimes necessary to form a stable bond between the resist and the desired substrate. The imprinting resists are considered the most critical elements for imprinting systems, and most of the NIL foundries have their associated imprinting resist optimized for the tool and process. Various resists have also been developed for applications, such as thermally curable polymer[71,73], particle-containing resin, fast-curing resist[74], etc.

With the direct patterning feature, NIL can process materials that are difficult to pattern by traditional optical lithography, including polymers, metals, and nanomaterials[73,75]. Intriguing devices can be built with a combination of functional polymers and nanoimprinting. Lin et al. demonstrated the highly sensitive ultrasound sensor by thermal imprinting optoelastic polymers to form microring resonators, as shown in Fig. 3(b-i)[54]. Much progress has been made since then. Lin et al. used soft NIL and a damascene process to fabricate all-polymer high *Q*-factor microring resonators, with images shown in Fig. 3(b-ii)[54]. Such a damascene structure can allow the backfill of functional materials for more diverse applications[54,76]. Lin et al. used thermal imprinting to form a template and ink-printing electro-optic polymers to make a polymer E-O modulator[77]. The light-emitting conjugated polymer was used as a gain medium and was shaped into a laser cavity to form nanolasers[78]. Ferroelectric polymers were also utilized to achieve non-volatile, low-voltage memory effects[79].

The development of non-organic nanoimprinting resist is active in both academia and industry. One of the motivations is to support emerging photonic applications and overcome the low refractive index limitation of polymer materials, thereby achieving versatile functionalities for applications such as augmented reality and flat optics. One common strategy is to incorporate high refractive index metal or metal-oxide nanoparticles, such as TiO_2[80] and ZrO_2[81] particles, into the polymer resist to form a hybrid composite resin. Based on the formulation, the hybrid composite resin can be spin-coated or inkjet-cast onto the substrate and be used for either T-NIL or UV-NIL. After imprinting, thermal annealing can be applied to further solidify the structure. The drawback of the method is that the refractive index is still limited due to non-full crystallization in this scheme[82]. In addition, the presence of NP results in a non-smooth structural surface, causing strong scattering[80]. A slight shrinking of the final structure can also be observed.

Sol-gel synthesis is another commonly used method for incorporating metal, inorganic, and metal oxide materials into nanoimprinting structures[83]. In this method, a sol-gel solution with a precursor is first prepared and stabilized in the alcohol solvent. Then, a controlled amount of water is added to initiate the formation of the colloidal solution. The solution is then spin-coated and pressed with the patterned soft mold at an elevated temperature to perform thermal imprinting, drying, and crystallization. Since the solidified sol-gel material may create stress on the mold, it is necessary to use the soft mold. Elevating to a higher temperature may be required to trigger shrinkage to facilitate the demolding process. Kim et al. demonstrated that by imprinting TiO_2 sol-gel solution followed by thermal annealing with different temperatures, the material phase of patterned TiO_2 and the refractive index can be tuned[82]. It is worth noting that the sol-gel-based method can result in substantial structure shrinkage (~30%) after the structure is thoroughly dried. It is also possible to combine the nanoparticle method and the sol-gel methods to form the new composite. It has been proven that a high percentage of NP can substantially reduce shrinkage, as shown in Fig. 3(c)[80].

Inkjet dispensing strategy

Spin coating can uniformly coat a resist layer on a substrate. However, the material utilization is very low, with only 2%

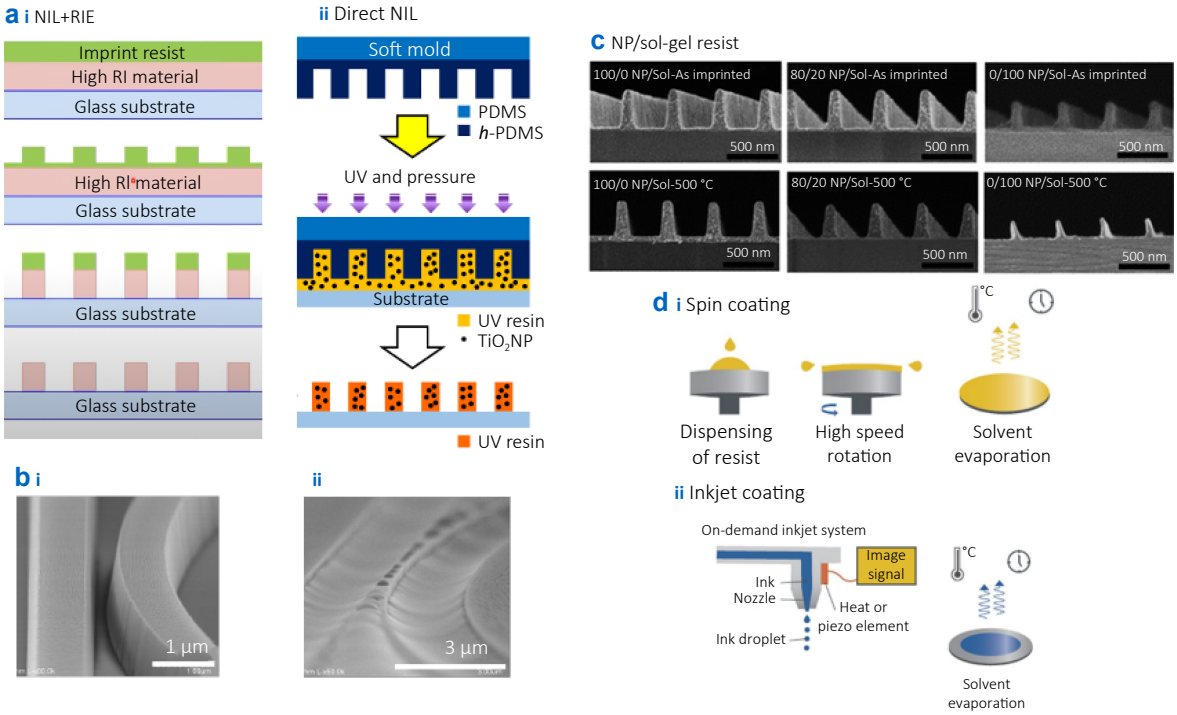

Fig. 3 | Imprinting resist in NIL. (**a-i**) Imprinting resist as the etching mask (NIL+RIE). (**a-ii**) Imprinting resist as the functional structure (direct NIL). (**b-i**) Polymer microring resonator (MRR) fabricated by direct NIL. (**b-ii**) Polymer microring resonator fabricated by damascene NIL process. (**c**) Images of fabricated nanogratings using NIL with inorganic resist composed of different percentages of sol-gel solution and nanoparticles. (**d**) Different types of resist dispensing methods. Figure reproduced with permission from: (a-i) ref.[85], SPIE; (a-ii) ref.[70], (b-i) ref.[54], (b-ii) ref.[54], under a Creative Commons licences; (c) ref.[80], American Chemical Society; (d) ref.[84], under a Creative Commons licences.

of the resist remaining on the substrate after the spinning[84]. Moreover, the non-uniform residual layer can happen after imprinting, degrading the pattern density. The inkjet dispensing method with a drop-on-demand strategy is developed to solve these issues. Figure 3(d) shows the comparison with these two methods[84]. In the inkjet dispensing method, the resist distribution can be adjusted based on the structures and the pattern density to compensate for the resist loading effect, achieving a uniform residual layer across the entire imprinted region. Additionally, the resist filling time can be reduced by modifying the distribution pattern, such as breaking larger features into segmented patterns to enhance filling speed[45].

Despite its advantages, the inkjet dispensing process can be time-consuming and requires specialized materials and tools. The resist must have low viscosity at room temperature and be compatible with an inkjet printhead. The dedicated inkjet dispensing setup requires precise machine controls, including printing position, dispensing volume, filtering, and particle management. Due to the high costs and complex setup, inkjet dispensing is mainly used to produce high-value devices requiring precise process controls, such as metalenses, augmented reality waveguides, and semiconductor devices[86,87]. This inkjet dispensing technology has been integrated into high-end imprinting systems[86,87].

Imprinting method

Plate-to-plate imprinting

Plate-to-plate imprinting is the first demonstrated nanoimprinting method, as Fig. 4(a-i) illustrates[88]. In this method, the mold and imprinted substrate are of comparable size and are pressed together by two flat, rigid plates, followed by UV curing or thermal embossing. This technique does not impose many restrictions on resist dispensing and is compatible with solid and soft molds, offering high process compatibility and flexibility. Plate-to-plate imprinting can be implemented on a small scale for proof-of-concept studies. It can also be used to imprint an entire 300 mm wafer or more extensive panel-size substrate for manufacturing purposes[89]. Additionally, it can be integrated with an alignment system to ensure < 1 μm overlay error. Plate-to-plate imprinting is widely used in the industry to manufacture wafer-level optical elements, such as lens arrays, followed by wafer stacking to form compact optical modules[90]. Many advanced tools with high-volume manufacturing records are already available[89,91].

Despite the simple operation, full wafer plate-to-plate nanoimprint lithography has a few significant disadvantages. First, directly fabricating a 12" or even larger template through E-beam writing can be costly. Therefore, the step-and-repeat method is typically required to make a large working template. Second, as the imprinting size increases,

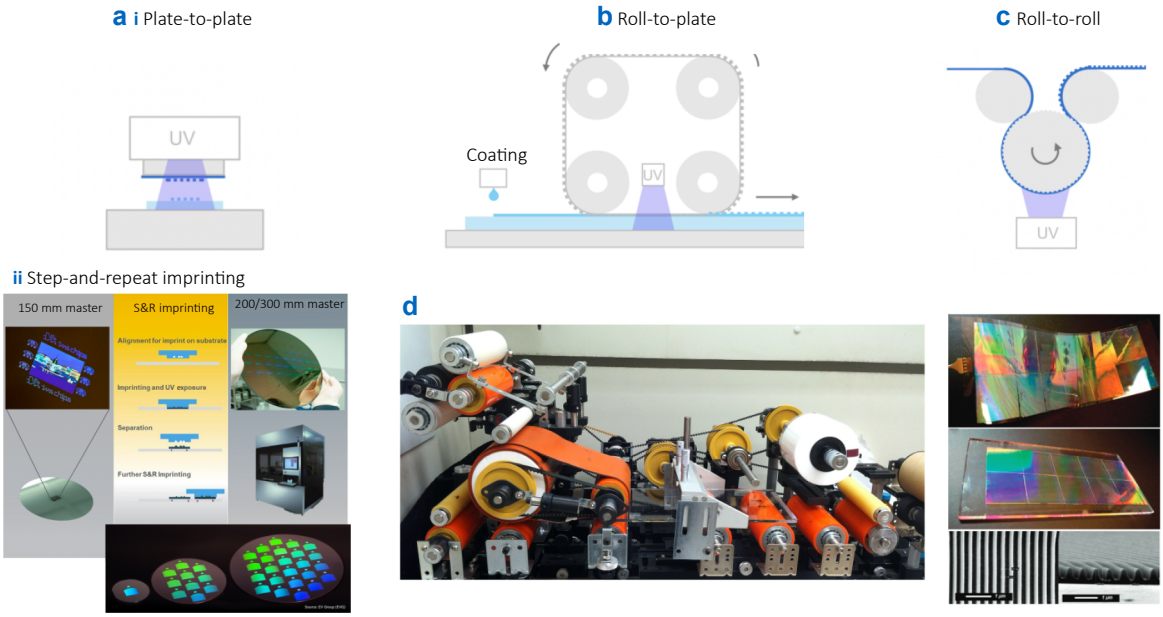

Fig. 4 | (**a-i**) Schematic diagram of plate-to-plate imprinting. (**a-ii**) Step-and-repeat imprinting. (**b**) Roll-to-plate imprinting. (**c**) Roll-to-roll imprinting. (**d**) Pictures of the roll-to-plate imprinting setup and the imprinted structures. Figure reproduced with permission from: (a-i, b, c) ref.[88], SPIE; (a-ii) ref.[92], SPIE; (d) ref.[88, 93], American Chemical Society.

NIL becomes more susceptible to defects, including repeated defects from foreign particles and random defects from air bubbles[44]. Ensuring uniform temperature and pressure control over the imprinting area is also challenging. The large contact area also requires larger forces to provide a suitable imprint pressure, which may exceed 20 kN over an 8-inch wafer[52]. To address this issue, soft molds are typically used in most modern imprinters for the whole wafer plate-to-plate imprinting. Third, the alignment to the underlying layer on the full wafer scale can be tricky since parasitic overlay errors increase with the field size[44]. Fourth, the full wafer plate-to-plate imprinting is not a continuous process, where the mold needs to be lifted and placed during each cycle, limiting the imprinting throughput.

Step-and-repeat imprinting

Instead of using a large mold to pattern the entire wafer, the step-and-repeat imprint lithography utilizes a smaller template that contains only a few dies to pattern the large wafer by imprinting it multiple times, as shown in Fig. 4(a-ii). This method significantly reduced the cost of preparing the mold. Moreover, a smaller area imprinting is usually easier and allows for better defectivity and overlay management[94,95]. The disadvantage is the lower throughput, which requires multiple imprinting to cover a large wafer fully. The step-and-repeat method has been extensively used for working stamp preparation, where a large working stamp can be obtained by imprinting multiple times on the same wafer[94].

Inkjet dispensing step-and-repeat imprint lithography is a notable advancement. It combines the advantages of both the step-and-repeat (smaller master mold, better quality control) and the inkjet dispensing method (thin and uniform residual layer), allowing NIL to achieve < 3 nm overlay error and tight process control suitable for the most critical applications[96]. However, it comes with a more complicated system than plate-to-plate imprinting. To enhance the throughput, multi-field dispensing, resist distribution optimization, and resist surface energy engineering are being implemented.

Roller-based nanoimprinting

Roller-based nanoimprinting is another widely used imprinting method, which starts with a continuous coating of the substrate with imprinting resist and then pressing the molding roller against the substrate for pattern formation[10,52,97]. The resist is cured using heat or UV exposure before it is finally detached from the mold on the other side of the imprint roller. The main advantage of roller-based imprinting is that it can achieve continuous imprinting by rotating the roller without the pressing and lifting process, boosting the throughput[19,98]. In addition, the contact area between the mold and the substrate is smaller, making it easier for imprinting control. The roller-based imprinting system can be further categorized into roll-to-plate and roll-to-roll nanoimprinting, as shown in Fig. 4(b, c)[88,98]. In roll-to-plate imprinting, the substrate is flat and is placed right in contact with the imprinting cylinder. As the roller rotates and the substrate moves forward with a corresponding speed, the pattern on the roller can be transferred onto the substrate coated with resist through the UV-NIL or the T-NIL with continuity. As for the roll-to-roll NIL process, an imprinting

roller with a patterned surface is used to imprint onto a flexible substrate on a supporting roller instead of a flat plate in roll-to-plate NIL processes, as shown in Fig. 4(c, d). The entire process is based on the roll-to-roll manufacturing concept, which has the advantages of high throughput and provides an up-and-coming solution for industrial-scale applications. It was reported that gratings of 70 nm lines were achieved using UV roll-to-roll NIL, with an imprint speed up to approximately 1,400 mm/min[52].

Despite the advantages, there are several challenges in roller-based nanoimprinting. First, the mold is not flat, and the pattern needs to be engraved on a cylindrical surface, incompatible with the traditional E-beam writing method. The easiest way is to use a flexible mold to wrap around the roller with sufficient flexibility, such as polyethylene terephthalate (PET) with polyurethane structures or electroplated Ni shim as a durable mold for large volume manufacturing. Second, the imprinting resist is usually thick, and the uniformity is difficult to control. To solve this problem, the inkjet dispensing method can be applied to allow better residual layer control[98]. Other concerns include the mold separation at the end of the imprinting process. The relative movement of mold to the imprinted patterns can cause a shear force during the demolding process and, therefore, is subject to pattern collapse defects for tall and high aspect ratio structures.

Challenges in NIL

Residual layer

Residual layers can pose significant issues for NIL, especially for critical dimension (CD) control and optical applications[86]. When the imprinted structure is used as the pattern transfer layer, the residual layer must be removed via plasma etching, which usually causes CD drift[99]. The final residual layer must be well controlled to achieve better process control. Minimizing the residual layer is crucial for photonic devices like AR waveguides, metalenses, and photonic integrated circuits[54,88]. The performance of the optical devices, including conversion efficiency, viewing angles, and quality factor, is highly contingent on the thickness of the residual layer and requires close attention.

One strategy for minimizing the residual layer is using the inkjet dispensing method, where the distribution of the resist droplets can be precisely calculated to avoid excessive resists that result in a thick residual layer[86]. As presented in ref.[100], when imprinting patterns with varying fill factors, such as slanted gratings with a nonlinear depth profile, the resulting residual layer thickness is usually thick and nonuniform. The measured residual layer thickness ranges from 308 nm to 377 nm. On the other hand, by using inkjet coating to create customized NIL polymer layers, the range of the residual layer can be decreased to 47 nm to 60 nm. Other strategies, such as self-assembly through heating[76], and the tape-assisted method to selectively peel off the residual layer without affecting the imprinted structures are also actively explored[101]. Additionally, residual layer-free imprinting was reported by using fast thermal-curable PDMS[102]. Making the structural height much greater than the residual layer for optical devices can relieve performance degradation and potentially impart other concerns. In some unique designs, the residual layer is used as an anti-reflection layer[59].

Defectivity

The high defect density is one of the significant obstacles to NIL for advanced applications. It can be divided into repeated defects and randomly distributed in the NIL process[44,103]. Repeated defects arise from mold errors due to mold damages or fabrication imperfections, leading to a repeatable error in each imprinting. Randomly distributed defects are not repeatable regarding location and mostly happen during resist filling or demolding. To tackle the repeated defect issue, operating NIL in a clean environment is necessary to prevent particles from falling on the surface. Resist filtering is needed to avoid the presence of crystallization and solid pellets in the resist solution.

Random defects can be further separated based on the defect morphologies and mechanisms, as shown in Fig. 5(a) and Fig. 5(b), respectively[44,95,103]. i) shows the feature distortion defects due to local shear stresses, resulting in the misalignment of the nanopillars. ii) demonstrates the cohesive failure defects with local structural breakage or pattern stripping from the demolding process. This occurs because of the weak adhesion force to the substrate. iii) features the collapse defects that are caused by low resist modulus, high aspect ratio pillars, or minimal spacing between pillars; iv) illustrates large-scale shear defects that are caused by fast and uncontrolled separation step, resulting in non-local resist delamination; v) shows incomplete filling defects that arise because of insufficient imprinting time or low mobility of the resists, and vi) depicts surface contamination voids defect with local dewetting spots, which is believed to be caused by airborne organic vapors that adsorb onto the adhesion layer[44].

Efforts have been made to study and alleviate random defect issues. Generally, the aspect ratio cannot be too high to avoid feature collapse. The imprinting resist should maintain high mechanical strength and adhesion to the substrate. Controlled motion is necessary during the demolding process[95]. The imprinting time must be set appropriately to ensure complete filling without sacrificing throughput. Imprinting conditions, such as purging gas, could also be essential in controlling void defects[104]. As described in ref.[95], the defectivity can be greatly reduced by optimizing the resist material and proper imprinting control for the semiconductor memory applications. By simply improving the material strength, including the tensile modulus, and reducing particulates in the resist, the defect density can be reduced by more than two orders of magnitude. By finely controlling the separation process and performing resist filtration system, the defect density can be

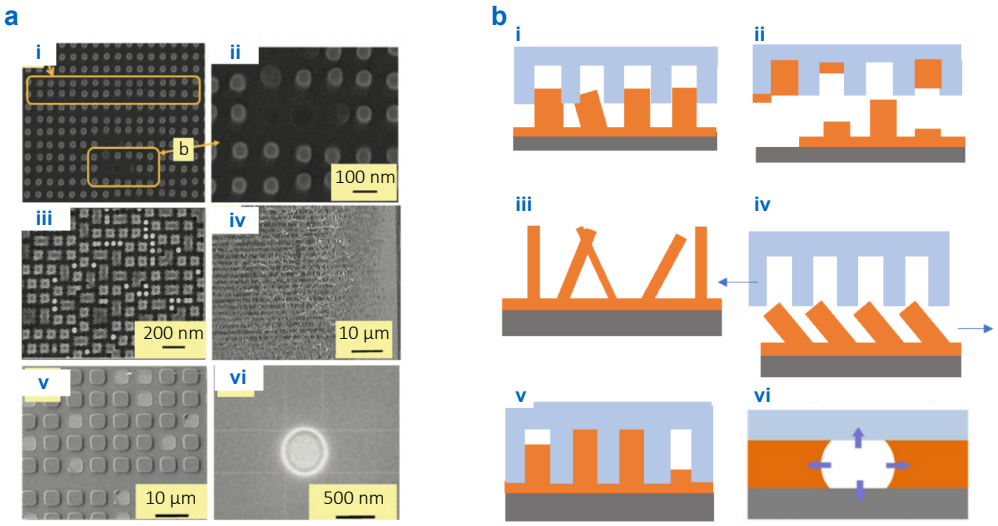

Fig. 5 | Defect images (**a**) and the mechanism (**b**) of common defect modes in the NIL. (i) Feature distortion, (ii) adhesive failure, (iii) feature collapse, (iv) large-scale shear defects, (v) incomplete filling, and (vi) surface contamination void defects. Figure reproduced with permission from ref.[44], under a Creative Commons licences.

decreased by another order. By storing wafers in a nitrogen environment prior to printing and by adding carbon filtration systems, the defect density can be further brought down by 60%.

Alignment and overlay control

The precise alignment of the current layer to the previously patterned ones is essential for making more advanced structures[105,106]. However, due to the configuration difference, the alignment method used in optical lithography cannot be applied to NIL, and a new alignment process must be developed. In the most advanced applications, the overlay error must be less than 3 nm to ensure the correct final device functionality and circuit connection for modern semiconductor manufacturing[96]. To satisfy this need, the high-order distortion, such as magnification errors resulting from the shape differences between the mold and the desired imprinting pattern, must be adjusted to minimize the overlay errors further.

Nanoimprinting for high-volume manufacturing

After 30 years of development, NIL has been used for manufacturing in various areas, such as semiconductors, augmented reality, biomedicines, displays, and optoelectronic devices. Compared with traditional photolithography utilized for mass production, it can achieve high-resolution patterning with a simple implementation setup. The CMOS-compatible feature also allows NIL to work with other well-developed patterning technologies, such as dry etching and lift-off processes. In addition, it can be manufactured at a large scale by using roller-based imprinting for relatively low-cost yet high-volume manufacturing purposes. It can be realized on a non-flat surface, catering to special needs for specific applications. The defectivity issue of NIL is one of the manufacturing concerns. These defect types have been studied and addressed in the past 30 years. Many applications have recognized NIL's quality and have been adopted in manufacturing.

As advanced applications such as semiconductors and meta-optics continue to push into the sub-50 nm and even sub-10 nm regime, high-resolution lithography has emerged as one of the primary bottlenecks in manufacturing. Among the available technologies, NIL, electron beam (E-beam) lithography, and extreme ultraviolet (EUV) lithography are currently the only viable candidates capable of meeting these demanding resolution requirements. While EUV lithography has been successfully implemented in leading-edge integrated circuit (IC) production, it comes with significant limitations. The high cost of ownership, driven by the need for complex and expensive systems —including high-power light sources, multilayer reflective mirrors, and vacuum chambers—remains a critical challenge. Additionally, EUV's energy consumption is a major concern. According to ref.[87,107,108], the power consumption of EUV is 10× higher than the NIL and 2× the cost per wafer in the patterning of 15 nm devices for semiconductor manufacturing[109]. In contrast, E-beam lithography offers excellent resolution but suffers from extremely low throughput due to its serial patterning method, where patterns are written point by point. This makes it more suitable for mask-making or research-scale prototyping rather than high-volume manufacturing. These limitations highlight the growing need for alternative lithographic approaches, such as NIL, which promises high resolution, lower energy consumption, and greater cost-efficiency for certain advanced applications.

Nanoimprinitng in semiconductor manufacturing

Semiconductor manufacturing is a highly complex and sophisticated process that demands exceptional stability and precision. For NIL to be viable in silicon IC production, several critical requirements must be met: i) imprinting resolution finer than the critical dimension of the structures; ii) overlay error meeting the required error budget of the application relative to the minimum half-pitch; iii) low process defectivity to ensure an acceptable defect density based on the applications; iv) high throughput with > 80–100 wafers/hr for a 300 mm wafer to ensure an acceptable run rate and a competitive cost of ownership of the tools.

In the early 2000s, several semiconductor companies attempted to adopt NIL for semiconductor manufacturing due to its exceptional resolution. However, as the technology was not mature enough, the defectivity, overlay, and throughput were far behind the semiconductor manufacturing requirements and were not considered a concrete solution for advanced semiconductor manufacturing. After decades of development, nanoimprinting suppliers, such as Canon Inc., have made significant progress in improving the NIL system and greatly enhancing the NIL quality to meet the stringent requirements of the semiconductor industry. In 2023, Canon Inc. announced their first semiconductor-graded nanoimprinting tool (FPA-1200NZ2C, Fig. 6(a-i)) for 12" wafer patterning and has shipped the tool

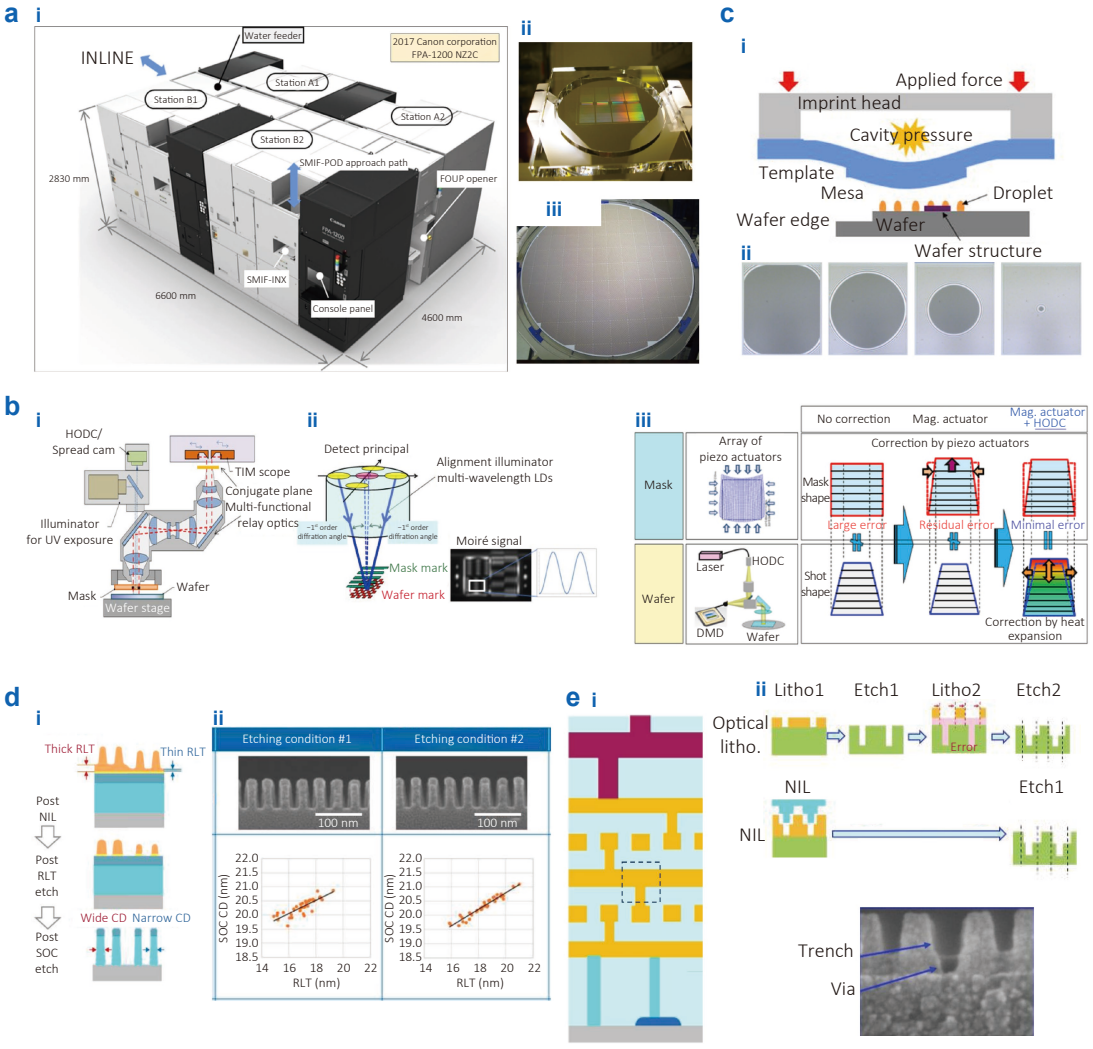

Fig. 6 | The first-ever semiconductor-graded nanoimprinting tool FPA-1200NZ2C by Canon Inc. (**a-i**) The appearance of the imprinting tool. (**a-ii**) The imprinting mold. (**a-iii**) The 12" wafer patterned by FPA-1200NZ2C. (**b-i**) The alignment detection scheme. (**b-ii**) Misalignment can be measured by detecting the 1st-order Moire fringe. (**b-iii**) Higher-order distortion can be compensated by pressing the stamp and applying laser heating to the wafer. (**c-i**) The template is bowed to produce a parabolic contact with the imprinting resist. (**c-ii**) The sequential images of the separation process. (**d-i**) The NIL imprinting and pattern transfer process schematic diagram. (**d-ii**) The etching condition and residual layer thickness (RLT) can effectively influence the CD of the underlying SOC layer. (**e-i**) The semiconductor interconnect layer in the semiconductor back-end-of-line process. (**e-ii**) The comparison of the damascene process by optical lithography and NIL. Figure reproduced with permission from: (a, c-i) ref.[44], under a Creative Commons licences; (b) ref.[96], (c-ii) ref.[95], (d) ref.[99], (e) ref.[110], SPIE.

to the foundry customers in 2024. According to ref.[87,109], the tool has satisfied the 20 nm 3D NAND requirements for both resolution and overlay requirements, and the high-volume manufacturing is under evaluation.

Semiconductor-graded NIL tool

The FPA-1200NZ2C is the first semiconductor-graded tool that meets the industry's requirements. It is a UV, inkjet coating based step-and-repeat imprinter targeted to work on 12" wafer manufacturing. The master stamp is made by Dai-Nippon Printing through E-beam writing on a 6" wafer (Fig. 6(a-ii))[44]. The working stamp strategy is applied to extend the lifetime of the master mold. The nominal imprinting linewidth is 14 nm, corresponding to 5 nm-node for the advanced logic semiconductors, and is expected to be able to pattern with a minimum linewidth of 10 nm, corresponding to 2 nm-node. The patterning field size is 26 mm × 33 mm, matching the typical field size of the optical lithography as shown in Fig. 6(a-iii)[44]. It is compatible with the 12" semiconductor wafer with imprinting throughput of 20 wafers/station and 80 wafers/tool. The nominal overlay accuracy is < 3 nm[109]. The reported average defect density of the tool by using the device-like patterned mask with 20 nm half-pitch line spacing is 0.03 defects/cm^2 [87]. This section will briefly overview how the first semiconductor-graded NIL was built and how improvements are made.

The alignment detection scheme of the FPA-1200NZ2C system is based on the interference effect where the imprinting mold and the alignment mark on the substrate form special Moire fringes under a specific illumination setting with multiple wavelengths, as illustrated in Fig. 6(b-i)[105]. By detecting the first-order interference pattern through the mask, mold misalignment can be detected with sensitivity down to 1 nm in accuracy. As for the alignment process, the coarse alignment with ~500 nm precision is done before the contact of the mold and the substrate[44]. After contact, adjustments are applied to fine-tune the rotation and lateral alignment. The high-order distortion error compensation is then done using two different approaches unique to NIL. The magnification actuation system uses multiple actuators that apply force to deform the mold for a better overlay. The distortion errors are also remedied by the high order distortion control (HODC), where the DMD mirrors are used to impart a laser to introduce localized heat on the substrate to cause deformation on the field-to-field basis, as shown in Fig. 6(b-ii). Other methods, such as mold tilting and force management, are also applied to avoid distortion errors[96,105]. So far, the average + 3 sigma matched machine overlay with ASML ArFi scanner was 2.4 nm and 2.2 nm in x and y. For the single machine overlay measurements (NZ2C to NZ2C), the average + 3 sigma in x and y was 1.8 nm and 1.5 nm, meeting the requirement for the 3D NAND flash market[87].

The defectivity reduction of FPA-1200NZ2C is done by reducing the repeated and random defects[5,78]. Ceramic materials with unique treatments, such as polishing, coating, and heating, are used as chamber material to lessen the particles generated by the tool and prevent sidewall degradation[95,103]. Other tool parts, such as gas nozzles, undergo mechanical and chemical polishing to flatten the surface. A high-filtration air curtain system is adopted to blow purified gas from the moving stage across the imprinting area to prevent particles from falling above the wafers[6,7]. Additionally, to prevent particles from being attracted to the imprint mask by the accumulated electrostatic charge during the demolding process, an electrostatic cleaning plate is used to compensate for the electrostatic potential generated on the imprint mask[103]. By applying these methods, the average repeat defect for each cycle has decreased dramatically from 10 pcs/wafer in 2013 down to 0.003 pcs/wafer in 2024[109,111].

The dominant random defects are the non-fill defects and the feature collapse. The non-fill defects can be minimized by ensuring sufficient imprinting time and avoiding trapping the air between the mold and substrate. As depicted in Fig. 6(c-i), micrometer-scale parabolic deformation of the template is generated by following a similar method in ref.[46] to create a convex contact surface to the resist drops during imprinting, resulting in a contiguous liquid film from the discrete drops without forming bubbles. The aspect ratio of the structure is limited to <2.5∶1 to avoid cohesive failure and pattern damage. The separation process is also well controlled to ensure a consistent speed during the process. Figure 6(c-ii) shows the authentic images of the separation process, demonstrating a uniform and symmetric separation front throughout 0.30 s[95]. In all cases, random defectivity was less than 0.03 defects/cm^2 and, for many instances, was well under 0.01 defects/cm^2 [87,109].

The low throughput of the step-and-repeat nanoimprinting is always a problem[95]. FPA-1200NZ2C uses strategies to address this issue, including improving the imprinting material wetting property, reducing the material filling time, improving the dispensing system, involving an innovative dispensing system, etc. The wetting property for the imprinting resist is engineered to be high so the material can spread and complete the resist filling quickly. Adjusting the resist dispensing system and reducing the single drop volume from 1.5 pL to 1.0 pL also decreases the required resist filling time[45]. Sparse patterns tend to fill more slowly because of the considerable distance between resist drops. This problem can be addressed by filling the area with dummy patterns. Over the years, sophisticated algorithms have been developed to search for the optimum drop volume and resist pattern to minimize the filling time and potential defects. When performing nanoimprinting, ambient gas can be trapped at the interface between the resist and the mold, forming micro-scaled bubbles. To facilitate the dissipation of bubbles, a gas permeable spin-on-carbon (GP-SOC) is used in the resist stack, which can

quickly take up the gas, resulting in a shorter spread time. Changing the ambient gas from He to CO_2 in the imprinting system was theoretically and experimentally proven effective to expedite the dissolving process.

The outstanding achievement of the FPA-1200NZ2C also comes from the establishment of a nanoimprinting ecosystem[87,109,112]. As an example, the defect control of NIL relies on the defect inspection system to accurately identify the defect failure modes and the source of failures[113]. The repeated defects during the imprinting can be quickly identified using an in situ mold inspection system. Implementing a master mold cleaning station can further reduce the defect density. It is also known that the resulting patterns transferred to the underlying layer depend on the nanoimprinted structures, residual layer thickness, descum method, and UV-curing dosage, as shown in Fig. 6(d). These factors are required to be well characterized and can be invaluable process knobs for critical dimension control[99]. The wafer flatness also plays a vital role in the imprinting quality. The improvement also relies on the improvement of planarization. Furthermore, similar to that in the current photolithography, a design rule needs to be established so that the engineers can design the layout accordingly to avoid potential failures from happening.

Semiconductor manufacturing status

The preliminary test data of NIL has met the standard for 3D NAND and DRAM applications in terms of defectivity, overlay, and resolution[87,109]. Several companies, including Kioxia[110], Toshiba[114] and SK Hynix[115], have been actively studying the feasibility of using nanoimprinting to pattern 3D NAND structures. Micron, one of the DRAM manufacturing companies, recently also announced the initiative to integrate nanoimprinting into its DRAM production processes, aiming to reduce production costs and enhance efficiency[116]. As for logic devices, Canon Inc. is dedicated to developing NIL technology for the back-end-of-the-line process at 12 nm half pitches and below for the metal interconnect process[87,109]. Due to the 3D patterning feature, NIL is expected to significantly simplify the dual damascene process for via-and-trench structure from several patterning steps and etching down to single patterning and one etching, providing a 40% less cost reduction, as shown in Fig. 6(e)[110]. Using NIL also intrinsically minimizes the overlay errors and the optical proximity correction issue due to the one-step process[83].

Even though NIL shows excellent potential for semiconductor applications, most of the reported works on NIL processes in semiconductor fabrication are still in the early path-finding phase, primarily aiming to evaluate NIL's process capability and compatibility. Therefore, continuous efforts are still needed to improve the tool and the process control. Cross-module cooperation is also necessary to optimize the process. For example, the 3D damascene patterning shows that the thinner imprinting resist can reduce the imprinting bubble defects[117]. However, this relies on the subsequent etching step to compromise for the thin resist. It is also worth noting that nanoimprinting will not wholly replace optical lithography but only substitute specific layers that show advantages by NIL.

Patterned magnetic nanostructures for hard disk drives

Conventional hard disk drives rely on granular recording media to store the information, but they increasingly suffer from data loss due to thermal fluctuations as grain size is reduced to achieve higher recording densities[3]. To address this limitation, the patterned magnetic nanostructures (PMN) approach has been proposed, in which a continuous magnetic layer is divided into an array of discrete magnetic dots—each representing a single bit. This strategy enables ultra-high-density storage and significantly improves thermal stability. However, the key challenge in realizing PMNs lies in fabricating these nanoscale dots with feature sizes around 10 nm and at densities exceeding 100 Gdot/in², all at a scalable and cost-effective manufacturing level[11].

To tackle this issue, the research team led by Stephen Chou pioneered T-NIL to offer ultra-high resolution, high throughput, and low-cost fabrication of nanostructures[12]. By using NIL, the team demonstrated a disc with a storage density of 400 Gbit/in², nearly three orders of magnitude higher than that of commercial disks and with 10 nm features and 40 nm periodicity[12,118]. Recognizing NIL's promise in data storage, several companies have initiated efforts to adapt NIL for commercial devices. For instance, Seagate Research Center has employed UV-NIL with inkjet coating to achieve dot patterning densities exceeding 2 Tb/in², using features as small as 18 nm[26]. Toshiba has also demonstrated a 2.5 Tb/in² bit-patterned media system using a self-assembly method combined with UV-NIL[27].

Despite these advancements, significant challenges remain. Mass-manufacturing of lithographically defined patterns requires precise control of pattern placement and tight tolerances across multiple disks to ensure consistency and functionality. Fabricating the NIL master mold with ultra-small feature sizes and high density is particularly demanding. Additionally, the pattern transfer process to the magnetic materials often involves etching, where maintaining size uniformity and structural fidelity becomes increasingly difficult as dimensions shrink[26]. These technical hurdles must be overcome to fully realize the potential of NIL-based PMNs in next-generation data storage.

Flat optics

Metalens has been one of the most exciting photonic technologies in recent years and is another leading force behind the development of nanoimprinting lithography. While metalens are small, they can behave like traditional geometric lenses. They can potentially replace the thick optical stacks in mobile phones, smart glasses, or even automotive

devices to realize multiple functionalities, such as facial recognition, dot projection for 3D sensing, image projection for lidar, image magnification, eye tracking, and ToF measurement[119].

As shown in Fig. 7(a-i), the metalens comprise arrays of nanopillars with < 100 nm feature size and high aspect ratio. When light passes through the meta-atoms with deep sub-wavelength feature sizes, light will experience a propagation phase shift, altering the field distribution. Precise light manipulation, such as light focusing, can be achieved by carefully engineering the structure and spacing of the pillars. The fabrication of metalens must satisfy

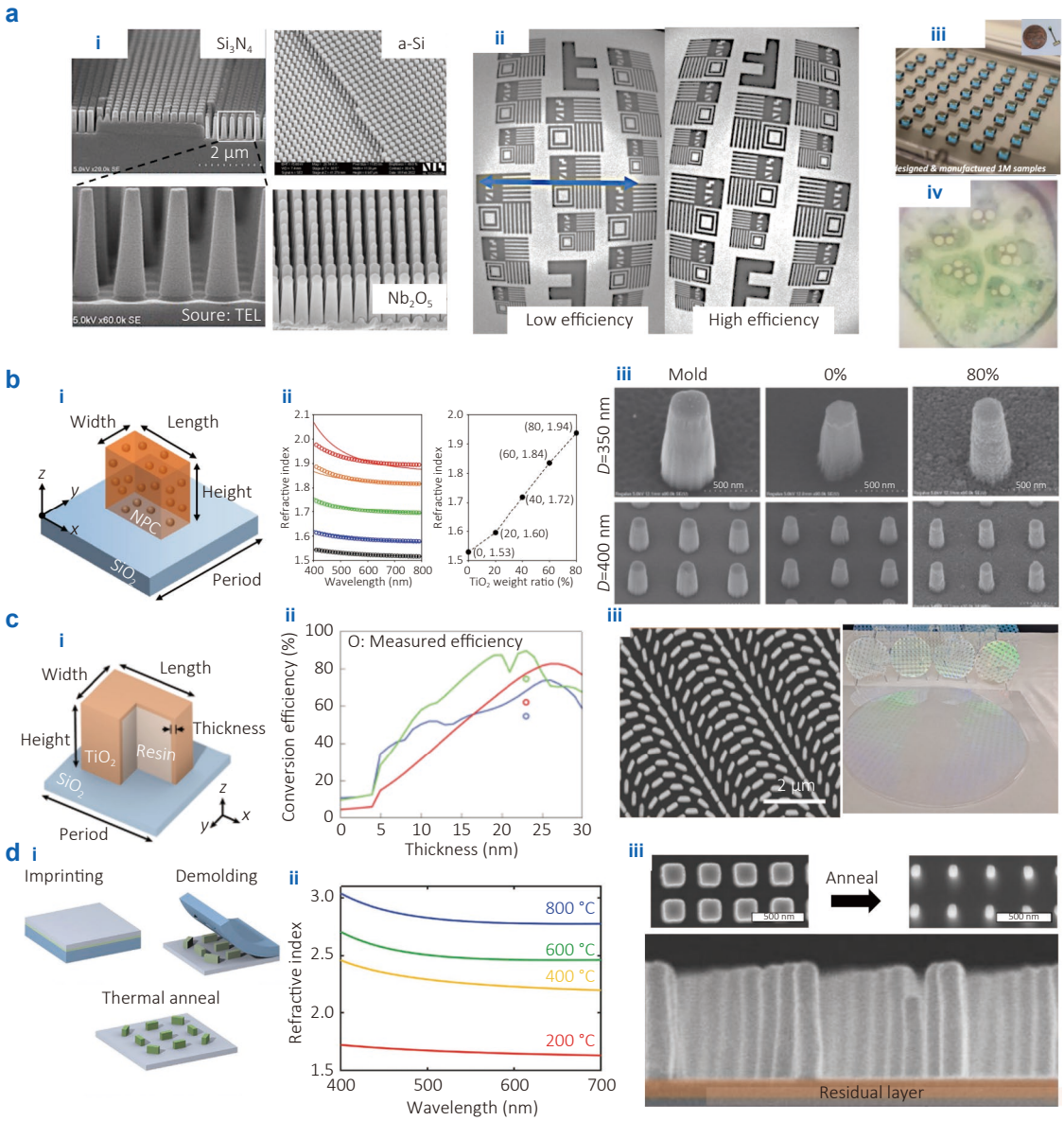

Fig. 7 | NIL for metalens manufacturing. (**a**) Metalens are made using the NIL + RIE method. (**b-d**) Metalens are produced by using the direct NIL process. (**a-i**) SEM images of the metalens made by different high-index materials. (**a-ii**) The comparison of images captured by metalens with high/ low diffraction efficiencies. The image of low-efficiency metalens shows a bright dot defect. (**a-iii**) The smallest camera modules using metalens produced by NILT. (**a-iv**) The magnified image of a pumpkin seed was taken by an iPhone and installed with an image magnifier metalens by Moxtek. (**b-i**) The meta-element formed by imprinting UV-curable resin mixed with nanoparticles. (**b-ii**) The refractive index can be tuned using different TiO_2 weight ratios. (**b-iii**) The surface roughness increases as the particle weight ratio increases. (**c-i**) The meta-element formed by UV-NIL followed by TiO_2 deposition. (**c-ii**) The metalens conversion efficiency increases as the deposited thickness of TiO_2 film rises. (**c-iii**) This method can be fabricated at a large scale. (**d-i**) The sol-gel imprinting process will be done with the post-annealing step. (**d-ii**) Higher annealing temperature results in higher refractive index due to the change of the crystal state. (**d-iii**) The nanopillars' shrinkage must be considered when designing the metalens. The residual layer is of a negligible thickness. Figure reproduced with permission from: (a-i) ref.[87, 121–122], SPIE; (a-ii, a-iii) ref.[121], (a-iv) ref.[123], SPIE; (b) ref.[70], under a Creative Commons licences; (c) ref.[124], Springer Nature; (d) ref.[82], under a Creative Commons licences.

several requirements to attain efficient and tight focusing by the metalens. First, the patterning resolution needs to be high with tight variation control. As discussed in ref.[120], a 5 nm variation in the nanopillars with 100 nm width can result in a >20% focus efficiency loss, which can lead to imaging artifacts such as "bright spots", as illustrated in Fig. 7(a-ii)[121]. Second, the pillar must be tall enough to complete a 2π phase control. It is typically greater than 500 nm for visible wavelength, and taller structures may be needed for longer wavelength. Third, the meta-structure composition requires high refractive index materials with low optical loss for better imaging conversion controllability. The commonly used materials are amorphous silicon (a-Si), Si_3N_4 for the NIR wavelength, Si_3N_4, TiO_2, and Nb_2O_5 for the visible wavelength, and ZrO_2[81] for the UV region. Fourthly, metalens with an area > 1 cm^2 are usually desired for better imaging quality and applicability.

The high resolution, high throughput, curved-surface compatible, and low-cost properties make nanoimprinting lithography one of the major technologies for manufacturing metalenses. Both the NIL + RIE and the direct NIL methods can be used for mass production with different advantages. The benefit of the NIL + RIE method is its high compatibility with the imprinting system that has been readily developed for the semiconductor industry. High patterning quality can be achieved. The main drawback is the requirement of high aspect ratio etching. Since the pattern density across the whole metasurface can vary significantly, the loading effect can greatly influence the etching profile and depth. In this regard, there are typically complete design rules for metasurfaces design to avoid layout issues. The residual layer thickness variation due to the varying filling factor across the lens area must also be considered. The deposition and etching of the thick (> 500 nm) high-index materials are usually time-consuming and require a dedicated method that may limit the process flexibility.

Several companies have verified the manufacturability of the metalens by using the NIL + RIE method. NIL technology (NILT) utilizes plate-to-plate NIL on a full wafer followed by dry etching to fabricate the 500 nm height a-Si-based meta-optical elements with excellent process control, as shown in Fig. 7(a-i)[125]. The three-sigma process variation of the fabricated meta-atoms with varying sizes on the lateral dimensions is 5 nm. As for the *z*-dimension, the height variation is ± 1 nm within the 2 mm field size and ± 10 nm for an entire 100 mm substrate. This tight process control enables the fabricated metalens to have a high focusing efficiency of > 80% and a slight variation of < 1.5%[126]. Recently, NILT has launched a series of compact metalens modules targeting different applications. The small form factor of the imaging modules can significantly benefit the wearable devices, as shown in Fig. 7(a-iii).

Moxtek is the first company to commercialize metalenses for visible wavelengths. As shown in Fig. 7(a-i)[122], their metalenses consist of Nb_2O_5 nanopillars with a high aspect ratio (> 12), tight peak-to-peak spacing (minimum = 70 nm), and a pillar height of 820 nm. The NIL process involves soft conformal imprinting lithography on a 200-mm glass wafer, followed by dry etching[122,123]. The produced metalenses exhibit an average of 86% focusing efficiency at the 532 nm wavelength and demonstrate high wafer-to-wafer consistency across multiple wafers (83%–90%)[122]. Additionally, the metalenses outperform geometrical lenses in terms of MTF when tested with green and red light. Recently, Moxtek launched products such as mobile phone magnification lenses and expanded its metalens foundry market. An example image captured with the magnification lens on an iPhone is displayed in Fig. 7(a-iv)[123].

On the other hand, the direct NIL method can pattern the imprinting materials into the final desired meta-structures without deposition and RIE steps[127]. One primary challenge is finding a suitable resist for imprinting, which must have a high refractive index (n>2.0) and low optical loss. Additionally, the structure must be physically stable to prevent drastic dimensional changes and strong enough to withstand the demolding process for tall structures. Recently, several advancements have been made to address issues regarding high scalability. Yoon et al. employed soft mold NIL to print metalenses functioning in the near-infrared region by mixing silicon nanoparticles with thermally printable resin to enhance the refractive index of the nanostructures[128]. Similarly, Einck et al. and Yoon et al. enhanced the refractive index of NIL resists by incorporating TiO_2 nanoparticles with UV-curable resin and successfully imprinted a meta-lens working in the visible spectrum, as illustrated in Fig. 7(b)[58,70]. Gong et al. utilized the commercially available resists composed of polysiloxane matrix and TiO_2 nanoparticles to fabricate metalenses working in the visible light range for anti-counterfeiting applications[129]. The use of polysiloxane instead of acrylate as the matrix provides low surface tension and better demolding properties, rendering imprinting patterns with aspect ratios exceeding 10∶1. Kim et al. reported the fabrication of centimeter-scale meta-lenses on a 12-inch wafer by depositing a thin layer of TiO_2 to compensate for the low refractive index of the resin, as shown in Fig. 7(c)[124]. Kim et al. used thermal annealing to modify the crystallization of the sol-gel structure, further increasing the refractive index beyond 2.5, as seen in Fig. 7(d)[82]. Common issues related to high-index materials include poor control over nanoparticle surface chemistry and size, leading to inadequate dispersion and larger particle aggregates that result in light scattering and haze. The shrinkage ratio of solvent-based resin is approximately 15% and needs to be minimized[83]. Other methods, such as patterning regular UV-resists followed by metal deposition, were also used to fabricate plasmonic metasurfaces for structural color and holographic encryption[130]. These plasmonic metasurfaces can also be implemented on a curved surface at a large scale[131].

Metalens through direct NIL is also actively developed in

industries to prepare for high-volume manufacturing. For example, Myrias Optics manufactures metalens by imprinting the TiO_2 composite resins described in ref.[58,80,132,133]. SolNIL is also actively developing a high-index imprinting solution for sol-gel-based metalens nanoimprinting[83].

Diffractive nanograting for augmented reality

The augmented reality (AR) glasses are another driving force behind NIL development, as illustrated in Fig. 8(a-i)[134]. In these AR glasses, a compact optical system is needed to convey light from distant displays to the user's eyes[92,135]. A widespread implementation is the diffractive waveguide system that uses high index substrate as the optical waveguide and the surface-relief gratings (SRG) structured on the substrate to diffract the light to couple in, expand, and outcouple from the source, as depicted in Fig. 8(a-ii). The typical SRGs include slanted and blazed gratings with ~100 nm feature sizes, tilted fins, and repeating periods of several hundred nanometers, as shown in Fig. 8(c)[136]. To provide a comfortable view, the area of the SRGs generally falls within the range of several square centimeters to accommodate the human eye boxes.

The key performance attributes of the diffractive waveguides include image contrast, luminosity uniformity, and field of view[137,138]. The material of the waveguide substrate and the grating structure plays a crucial role. As illustrated in Fig. 8(b-i)[139], high refractive index materials for both the waveguide and the grating structure strongly correlate to the display's field of view. The transparency of the waveguide material is equally important. Fig. 8(b-ii)[134] shows that using low-transparency material for the waveguide can reduce image contrast compared to using highly transparent waveguide materials. Additional factors must also be optimized, such as corner sharpness and side wall smoothness. Although the feature size for the nanograting is not as small as that in the metasurfaces, the process tolerance may be even tighter because light must propagate through the waveguide over a long distance. For instance, according to

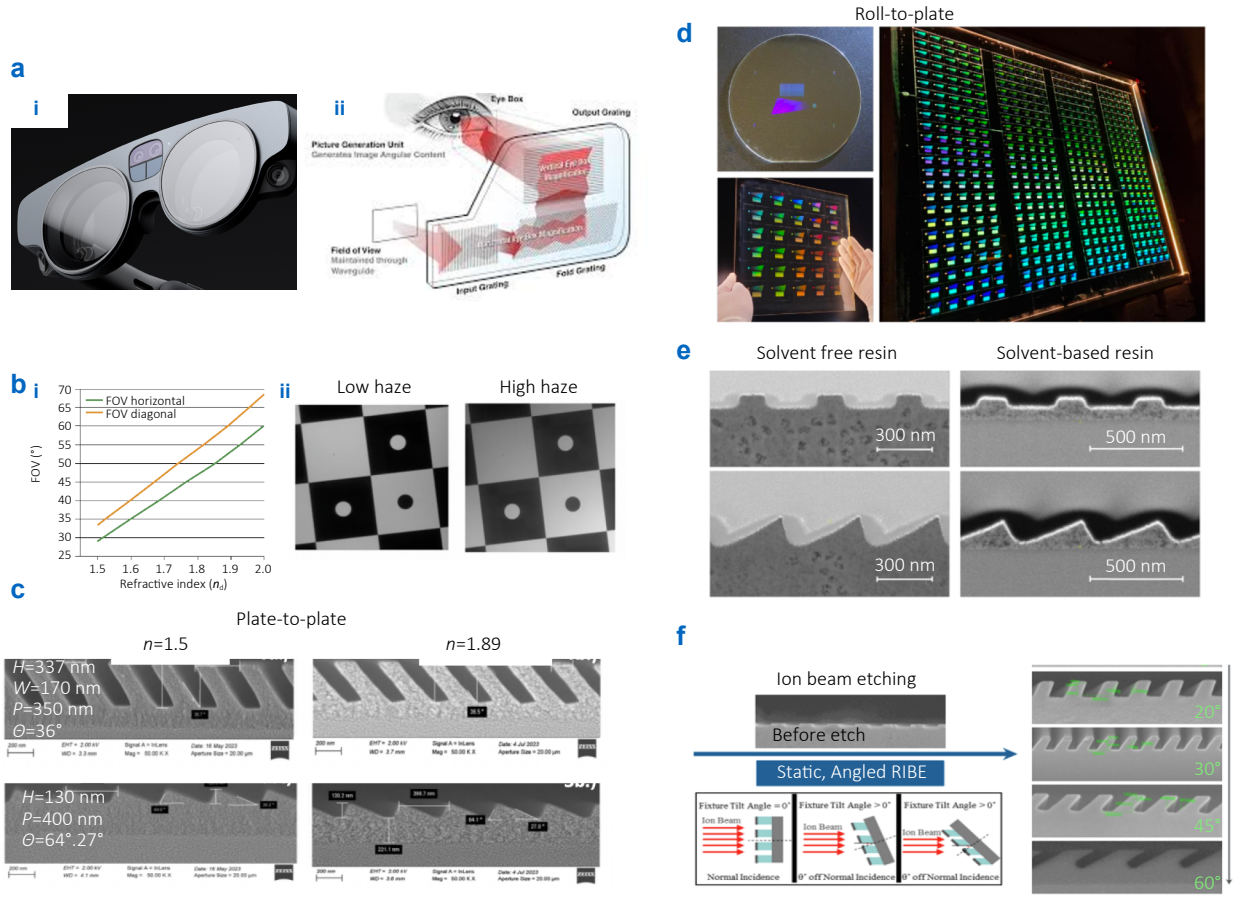

Fig. 8 | Nanoimprinting lithography for AR diffractive waveguide manufacturing. (**a**) Images of the Magic Leap AR glasses (a-i) and the light propagation within the AR glass (a-ii). (**b**) The refractive index and the transparency of the resin can influence the field of view (b-i) and the image contrast (b-ii). (**c**) The SEM images of the fabricated gratings with the standard resin (left) and the high index resin with nanoparticle fillers (right). The images show high resemblance and low shrinkage. (**d**) The AR diffractive waveguides fabricated by roll-to-plate imprinting with high throughput. (**e**) The SEM images of the fabricated gratings by roll-to-plate imprinting using solvent-free and solvent-based resin. (**f**) The etching method to fabricate the 3D slanted gratings. Figure reproduced from: (a-i) ref.[134], SPIE; (a-ii) Digilens, (b-i) ref.[139]; (b-ii) ref.[134], SPIE; (c) ref.[136], (d, e) ref.[88], (f) ref.[142], SPIE.

current industrial standards, the manufacturing tolerance for the grating period is on the scale of a few tens of picometers. For the tilted angle of the grating, it is on the scale of a few tens of arcseconds[137].

Multiple companies are working on manufacturing AR glass through direct NIL. Imprinting materials with high refractive indices, low haze (0.1%), high transparency (95%), and low shrinkage are under active development for AR diffractive waveguide applications[140,141]. Figure 8(c) shows the fabricated SRG structures using plate-to-plate NIL with an inkjet dispensing function[136]. The grating fabricated using nanoparticle-doped high-index composite resins shows similar results to those produced using UV resin. Despite the presence of the nanoparticles, the grating structures and the edges are still clearly defined[104]. The residual layer is also thin, with ~30 nm. The diffractive waveguides are also manufactured through roll-to-plate NIL[88,137]. Figure 8(d) shows a panel with 1100 mm × 1300 mm and 480 sets of waveguides in minutes using Morphotonic's roll-to-plate method[88]. The measured process variation of the fabricated grating periods is 20 pm, and the standard deviation of the relative orientation is 5 sec with tight process control. Despite the high throughput advantage, the thick residual layer (4.6 μm) is one of the concerns for the roll-to-plate imprinting, as illustrated in Fig. 8(e). This can be improved using lower viscosity solvent-based resin or optimizing the resist dispensing strategy. Pure polymer materials with a refractive index of 1.8 are also available on the market, providing high transparency in the visible wavelength[143]. NIL + RIE methods are also used to manufacture waveguide grating structures. By using the angled reactive ion beam etcher to etch the high index substrate, as shown in Fig. 8(f)[142], 3D SRG can also be achieved. The benefit of the NIL + RIE method is that it can be more compatible with high-index substrates such as SiC. However, it requires delicate tools and will limit the throughput[144].

Magic Leap is one of the pioneering companies that has successfully launched its AR glasses (Magic Leap 2) products, manufactured by NIL, as shown in Fig. 8(a-i). Magic Leap utilizes the inkjet dispensing method, combined with the roll-to-plate imprinting tool, to achieve high-throughput fabrication of SRGs with thin residual layers (10-20 nm). It also optimizes its imprinting tools to achieve double patterning on both sides of the waveguide glass. It uses up to 32 distinct depths for diffractive optical element design to achieve the desired functionalities. By optimizing the design and fabrication process, Magic Leap can achieve >90% yield with >2.0 process capability index, marking an exceptional process control and high uniformity of their roller-based NIL system. The resulting Magic Leap AR glasses demonstrate a 7× improvement in eye box efficiency and a 2× increase in outcoupling area compared with its previous version[134].

Wafer-level optics and wafer stacking

Manufacturing wafer-level optics for optical modules, such as LiDAR, face-ID, and image sensors, is another essential application for nanoimprinting lithography[145,146]. The basic idea is to use nanoimprinting to fabricate individual optical elements, such as optical diffusers, microlens, and diffractive optical elements, at the wafer level. These fabricated wafers are then aligned and bonded through UV bonding, forming a wafer stack. The wafer stack is then packaged with other elements, such as CMOS sensors and lasers, and finally is diced into individual devices. Due to the small form factors and lower cost-to-performance ratios, wafer-level 3D sensors and imaging systems have been widely used in automobile devices. Wafer-level UV imprinting of micro-optical components has become the first high-volume manufacturing application of nanoimprinting lithography since its introduction in 1995[147].

Microlens array is one of the most widely used wafer-level optics elements, as shown in Fig. 9(a, b-i) . High-quality, reliable, low-roughness microlens fabricated by UV-NIL technology have been commercialized using tailored UV resins for various applications[148]. The microlens array can be bonded with the CMOS sensors with high alignment accuracy to focus the incident light onto the active area of each sensing pixel, effectively enhancing the camera sensitivity. Diffractive optical elements and optical diffusers are widely used elements for beam shaping, as shown in Fig. 9(a, b-ii). By properly designing the structure, the output light can be altered into different shapes, such as discrete 3D point clouds, uniform top-hat beams, or a non-glare uniform illumination. Because the light conversion efficiency and the diffracted angle are highly related to structures of the diffractive elements, the NIL can provide unique advantages of 3D patterning and a better performance. By incorporating the diffractive elements with optical elements, such as laser, spacer, wire-grid polarizer, and filter, a compact optical module can be obtained for 3D sensing, lidar, and ToF sensors[149].

Recently, NIL has been extended to the wafer-level Si photonics packaging[150,151]. As shown in Fig. 9(c-i), a 3D polymer waveguide, a turning mirror (M1), and a curved mirror (M2) are fabricated through UV-NIL followed by metal deposition. The mirrors are used to direct the incident light to focus on the polymer waveguide. The imprinted polymer waveguides are 3D tapered from a cross-section of 11 μm × 11 μm to 5 μm × 2 μm and serve as mode converters to convert the large input beam into a smaller size to match the mode of the Si waveguide. The 3D tapered polymer waveguide is aligned along the underlying Si waveguide with sub-μm precision to facilitate the light transfer from the polymer waveguides to the Silicon ones, as depicted in Fig. 9(c-ii).

Display

Nanoimprinting lithography is used in display manufacturing. One famous example is the moth-eye-like structure, a

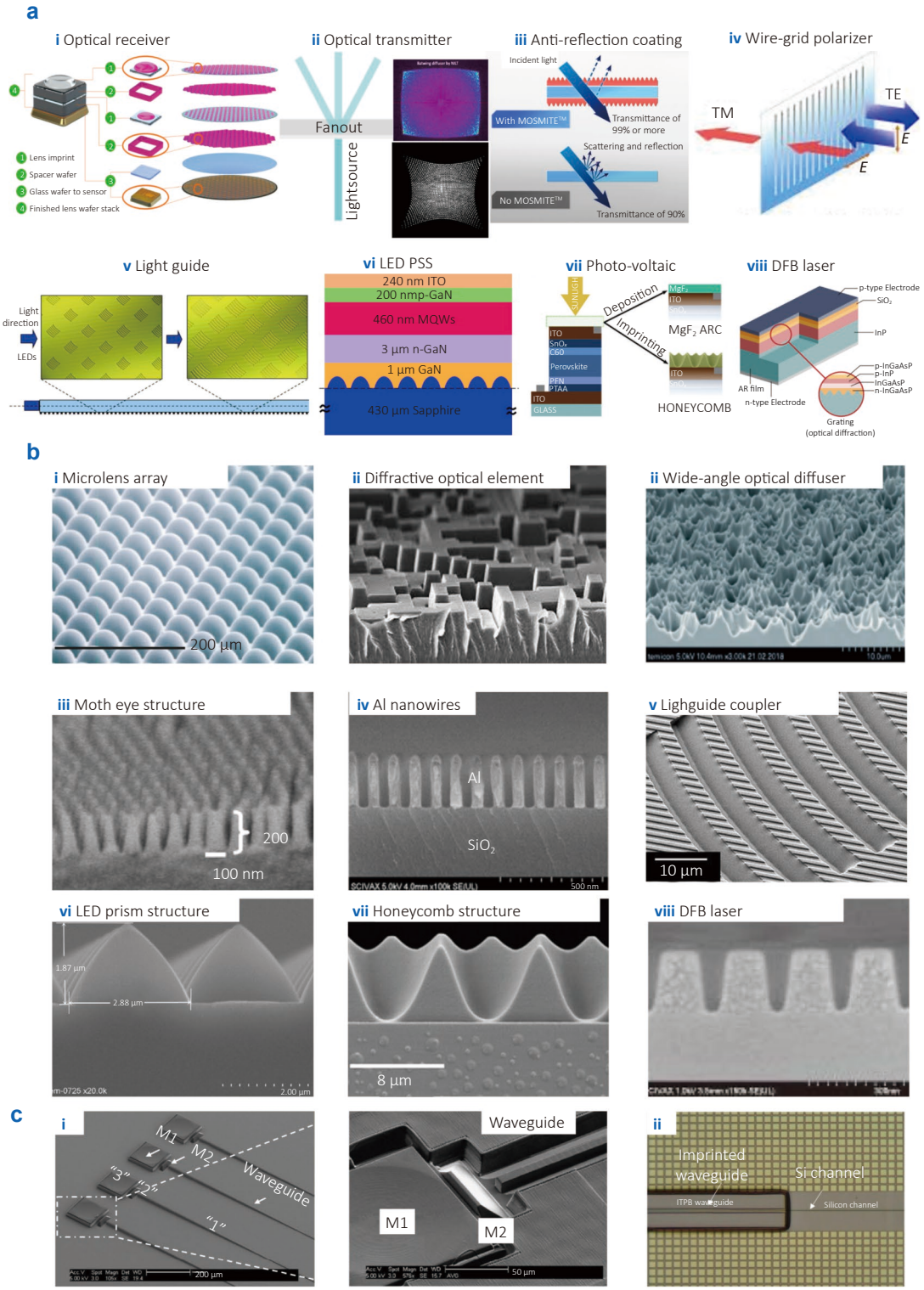

Fig. 9 | NIL for micro-, nano-optical device manufacturing. (**a**) The schematic, and (**b**) the representative structures of these applications. These applications include (**a-i**) optical receiver modules, (**a-ii**) optical emission modules, (**a-iii**) anti-reflection coating, (**a-iv**) wire grid polarizers, (**a-v**) light guides, (**a-vi**) LED patterned sapphire substrates, (**a-vii**) photo-voltaics, and (**a-viii**) DFB lasers. (**c**) NIL for wafer-level Si photonics packaging. (**c-i**) Nanoimprinted polymer waveguide and two reflective mirrors (M1 and M2). (**c-ii**) The polymer waveguide is imprinted on top of the Si waveguide with sub-μm alignment accuracy. Figure reproduced with permission from: (a-i, b-i) ref.[148], SPIE; (a-ii, b-ii) NILT websites; (a-iii, b-iii) Mitsubishi Chemical Group[152]; (a-iv, b-iv) Moxtek[153]; (a-v, b-v) ref.[154–155], Springer Nature; (a-vi, b-vi) ref.[90], under a Creative Commons licences; (a-viii, b-viii) Scivax[156]; (c) ref.[118].

bio-inspired structure containing dense pillars with 100–200 nm feature sizes, as shown in Fig. 9(a, b-iii) [152]. The moth's eye structure can be used as anti-reflection coating, substantially suppressing the light reflection from a glass surface from 8.0%-10.0% down to less than 0.5% with a broadband working wavelength. In addition, the unique structure also repels water, resulting in an anti-fogging and anti-water surface. These structures are now used in display, automotive, and exhibition windows and are mass-produced by plate-to-plate and roller-based imprinting[152,157]. Nanoimprinting is also used to make the aluminum wire grid polarizer, where linear aluminum lines with 50–100 nm pitches and 100 nm height are formed on a transparent substrate, as shown in Fig. 9(a, b-iv)[153]. The wire grid polarizer can be manufactured through the roll-to-plate or plate-to-plate method by patterning the etching mask and then etching the aluminum nanowires or by imprinting the polymer nanowires and then depositing the aluminum materials[158]. Since the wire grid polarizers are reflection-based, they can avoid optical loss compared to other absorption-based polarizers and show broader working wavelengths. They are used in high-brightness liquid crystal displays. It can also be integrated with wafer-level optics and bond with other optical elements for complex imaging applications[159]. Nanoimprinting is also used to fabricate structured light guide devices to create uniform illumination in the display technology. As shown in Fig. 9(a, b-v)[154,155], when the LED light enters the waveguide through the edge, the light will be trapped inside the waveguide until encountering the output coupling structures that are imprinted on the surface and emitting toward the display. These outcoupling structures are typically binary diffraction gratings, prism-like mirrors with 3–5 μm feature sizes. A thin and uniform-brightness display can be achieved by appropriately arranging the density and distribution of the structures. This structured light guide device has been adopted to illuminate displays, such as liquid crystal (LCD) based tablets and electronic ink readers[160].

Optoelectronic devices

Nanoimprinting is used in optoelectronic devices, such as light-emitting diodes, photovoltaic solar panels, and distributed feedback lasers. It has been shown that using a patterned sapphire substrate (PSS) for the GaN LED fabrication can substantially enhance light extraction efficiency (>30%), facilitate the epitaxial growth of the GaN LED, and enhance the yield[161], as shown in Fig. 9(a, b-vi)[90]. However, the sapphire substrates' rough and warpage nature make them difficult to pattern through traditional photolithography. These challenges can be significantly relieved by using full wafer-scale plate-to-plate imprinting with flexible molds followed by dry etching. Nowadays, NIL tools dedicated to patterning the PSS have been available and are gradually adopted in the LED manufacturing industry. NIL has emerged as a practical method to enhance the performance of photovoltaic devices. UV-NIL has been used to replicate periodic light-trapping geometries, such as pyramids, gratings, and meshes, on the front or rear electrodes of the thin-film photovoltaics to increase the effective path length of light through the active area to enhance the absorption and conversion efficiency of sunlight to electricity, as shown in Fig. 9(a, b-vii) . The high throughput nature of NIL can be an ideal tool for large-area photovoltaic devices. In addition to effectively increasing the absorption path length, NIL can control molecular orientation/crystallinity and enhance the deposition yield[161]. Nanoimprinting is also used to pattern the grating structure of the distributed feedback (DFB) laser, where the grating structure determines the feedback strength and the optical loss, as shown in Fig. 9(a, b-viii)[156]. Recently, IQE announced the adoption of using NIL to fabricate the periodic grating structures with ~500 nm period and low roughness and high quality in the DFB lasers[162].

NIL for fiber optics

Besides patterning planar structures on a large scale, NIL can create delicate patterns on tiny fiber tips (~10 μm for the core diameter) with high efficiency and cost-effectiveness. To pattern nanostructures on the fiber tips, an optical fiber is immersed in the UV-curable resin and aligned with the working mold through a piezo stage. After alignment, UV light was then coupled to the fiber to cure the resin, followed by a demolding process[163,164]. This method can quickly transfer patterns such as campanile probes for near-field super-resolution imaging[165], Fresnel lens for light focusing[166], top hat beam shaper, and vortex phase plates onto the optical fibers without dedicated tools, such as ion-beam milling, 2-photon polymerization, laser processing, etc. This fiber-based nanoimprinted technology is now being developed in preparation for volume production[167,168].

Biomedical applications

In addition to photonics and semiconductors, the application of NIL in the broader field of biomedical applications is growing rapidly, especially in gene sequencing[169]. In sequencing-by-synthesis (SBS) platforms, NIL reproducibly stamps arrays of uniform nanowells (≈100 nm diameter) into glass or polymer substrates, creating discrete reaction chambers for bridge-amplified DNA clusters. During sequencing, fluorescently labeled nucleotides are incorporated one base at a time into each well, and high-resolution optical imaging records each incorporation event. NIL also underpins the fabrication of solid-state nanopore sensors: it patterns 20–50 nm apertures in thin membranes, which can be thermally or chemically shrunk to single-digit–nanometer pores. When an electric potential drives single-stranded DNA through these pores, each nucleotide produces a characteristic blockade of the ionic current; real-time analysis of these current fluctuations then reveals the underlying DNA sequence. Several biomedical

companies, such as Illumina, have adopted NIL to manufacture DNA sequencing tools.

NIL is also useful for drug delivery applications, where nanoparticles with specific shapes and sizes can be precisely engineered. By using a precursor solution containing cross-linkable polymers and biomaterials in combination with predefined molds, highly monodisperse, enzymatically responsive nanoparticles as small as 50 nm can be fabricated[170]. NIL can also be used for immunoassay chips and nanofluidic chips for biosensing and analysis[171,172]. As an example, by precisely controlling the cross-section of the nanofluidic channels from 300 nm × 700 nm to 75 nm × 120 nm, the stretching state of DNA flowing through the nanochannels can be modulated[173]. In tissue engineering, NIL is being explored to create biomimetic surfaces that guide cell growth and behavior[174,175]. Other applications, including direct protein patterning at the nanoscale, have also been demonstrated[176].

Research development in academia

Besides industry and manufacturing dedicated to optimizing the imprinting system and process for volume production, academics are more focused on exploring new nanoimprinting applications and leveraging NIL's advantages to improve the capability. Thanks to the fewer material constraints of NIL, many materials can be patterned with NIL, and new properties can be found. In addition, since NIL usually involves heating and pressing steps, functionality can be different. Researchers are also actively investigating methods to solve the intrinsic challenges of NIL, such as residual layer issues and demolding-induced defects. Variations of NIL, such as ultrasound-assisted NIL, are also leveraged to make NIL broadly applicable in different areas.

High-quality factor optical devices

One significant advantage of NIL is the low lithography-induced edge roughness, which makes it suitable for fabricating high-quality integrated photonic devices. In the optical waveguides, the optical scattering induced by the waveguide roughness is the dominant factor that causes light dissipation. The waveguide roughness can be generally separated into line edge and sidewall surface roughness. The former usually occurs during the lithography step, where the dosage fluctuation or insufficient resolution of the lithography are the major contributors. The latter usually results from the etching process, causing a non-smooth sidewall. Even though the feature size of the optical waveguides is only a few hundred nanometers, the performance of the photonic integrated circuits is sensitive to the nm-scaled roughness. NIL can substantially avoid the roughness issue because the fabrication of the NIL mold is typically based on the E-beam writing, where the lithography-induced roughness can be minimized. In addition, NIL mold is typically fabricated on standard materials, such as Si or SiO_2, with mature etching technologies.

Using thermal imprinting with a highly smooth Si-mold, Lin et al. fabricated polymer microring resonators with a quality factor > 1.5 million on the thin polystyrene films (n= 1.58) on a full wafer scale[54]. Compared with other polymer devices, the quality factor is 1−2 orders higher when using NIL. Nanoimprinting can also fabricate high-quality factor devices through NIL + RIE methods. Liu et al. demonstrated that using the pattern transfer layer, the Q-factor can reach higher than 10,000,000 for SiN microring resonators. The fabricated devices have been used for nonlinear optics to generate a high-quality frequency comb[177]. The NIL can also be used for high Q-factor 3D devices. Ofer et al. used direct laser writing to pattern a master mold of micro-resonator in 3D, followed by dual soft NIL with PDMS and SU8 curable resin to transfer the pattern into the sol-gel materials[178]. To reduce the surface roughness inherited from the direct laser writing, a thermal reflow step was performed in the middle of the dual imprinting to smoothen the defects, as shown in Fig. 10(a-i). The thermal reflow technique boosted the measured Q-factor from 110,000 to over 3,000,000, as illustrated in Fig. 10(a-ii). This work demonstrates the high Q-factor 3D nanophotonics devices by using simple apparatus.

Molding-induced molecular alignment

NIL provides a unique manner to control chain alignment and crystal orientation in semi-crystalline polymers. Cox et al. and Aryal et al. demonstrated the capability of controlling the 3D chain alignment of the conjugated polymer poly(3-hexylthiophene) (P3HT) by using T-NIL[75,179]. During the imprinting process, polymer chains tend to align along the polymer flow direction. The P3HT molecular chains rotate during the high-temperature process and turn toward the hydrophobic sidewalls of the mold due to the interaction of the hydrophobic mold surfaces, as shown in Fig. 10(b-i)[179]. By using different mold structures, such as 1D nanograting and nanopillars, the polymer chain can be effectively modulated and aligned, as shown in Fig. 10(b-ii). Since the polymer backbone is related to the carrier transport property, this capability has recently been engineered to improve the performance of solar cells and field effect transistors (FET).

Hu et al. demonstrated the capability of modulating the orientation of ferroelectric polymer crystals when using properly designed molds for T-NIL[180]. After imprinting, the orientation of the chain axis that the dipole moment rotates about on application of a vertical electric field is aligned parallelly to the substrate with high uniformity, leading to a low-voltage operation. The preferential orientation of the crystals in the ferroelectric nanocells greatly enhances the performance of the ferroelectric polymer memory devices, enabling them to compete against more expensive technologies such as flash memories.

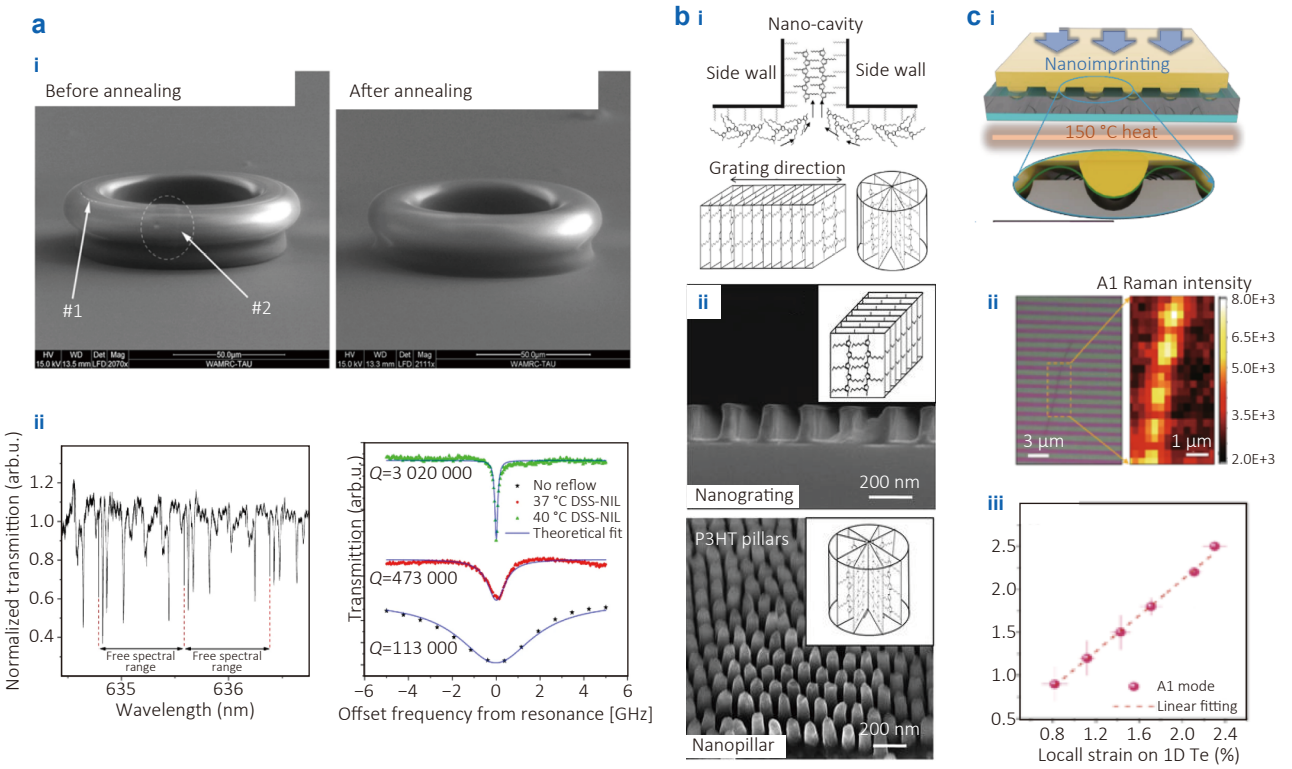

Fig. 10 | NIL imprinting in the research area. (**a-i**) SEM images of the 3D micro-resonator fabricated by NIL. By applying annealing, the defects on the surface can be reduced. (**a-ii**) the measured spectrum under different annealing conditions. (**b-i**) NIL is used for polymer molecular chain alignment. (**b-ii**) By using different molding structures, polymer molecular chain direction can be modulated. (**c-i**) Strain engineering is done by using T-NIL. (**c-ii**) The induced strain can be seen using Raman spectroscopy. (**c-iii**) The Raman shift is proportional to the local strain. Figure reproduced with permission from: (a) ref.[178], under a Creative Commons licences; (b) ref.[179], American Chemical Society; (c) ref.[181], under a Creative Commons licences.

Pressing for strain engineering

Strain engineering is a promising method to modulate material properties and device performance, such as carrier mobility, conductivity, and band gap modulation[180]. The nanoimprinting process, which involves pressing and heating, can effectively engineer materials with nanoscale resolution. Wang et al. demonstrated that by stamping the mold with periodic gratings onto the substrates with Te nanowires, a periodic strain field can be induced, altering the optical properties of the Te nanowires, as illustrated in Fig. 10(c-i)[181]. The observed Raman spectra reveal the strong lattice vibration response under the corresponding strain conditions, suggesting the potential of 1D Te as a promising candidate for deformable optoelectronics and wearable sensors, as illustrated in Fig. 10(c-ii) and Fig. 10(c-iii). Sun et al. demonstrated the capability of strain engineering in 2D materials at low cost[180]. Continuous tuning of the strain magnitude and generating various strain distributions of 2D materials were successfully achieved and evaluated by scanning Raman spectroscopy. This strain engineering method is compatible with standard semiconductor fabrication processes, providing prospects for advances in broad nanoelectronic and optoelectronic devices.

Different types of NIL

Polymer fiber imprinting

Most nanoimprinting technologies are implemented on flat or semi-flat substrates. Recently, a directly imprinting thermal drawing (DITD) technique demonstrated the capability of patterning on the entire fiber surface with a ten-nanometer resolution and a large scale, as shown in Fig. 11(a)[182]. In this process, a polymer preform (PVDF) was fed into a furnace to elongate the preform into a thin fiber. It is then passed through a pair of rollers with the desired surface structure to transfer the pattern from the mold onto the fiber with high resolution. It is a continuous process that enables large-scale, high-resolution polymer imprinting, such as grating structures. The plasmonic effect can be observed by depositing a thin gold film on the imprinted nanorod structures on the fiber, which is expected to be useful for biosensing applications. The technique also shows compatibility to pattern other functional fibers and can be used for self-powered wearable multi-point touch sensors.

Laser nanoimprinting

Nanoimprinting can also directly pattern hard materials, such as crystalline Si and metal with nanometer resolution.

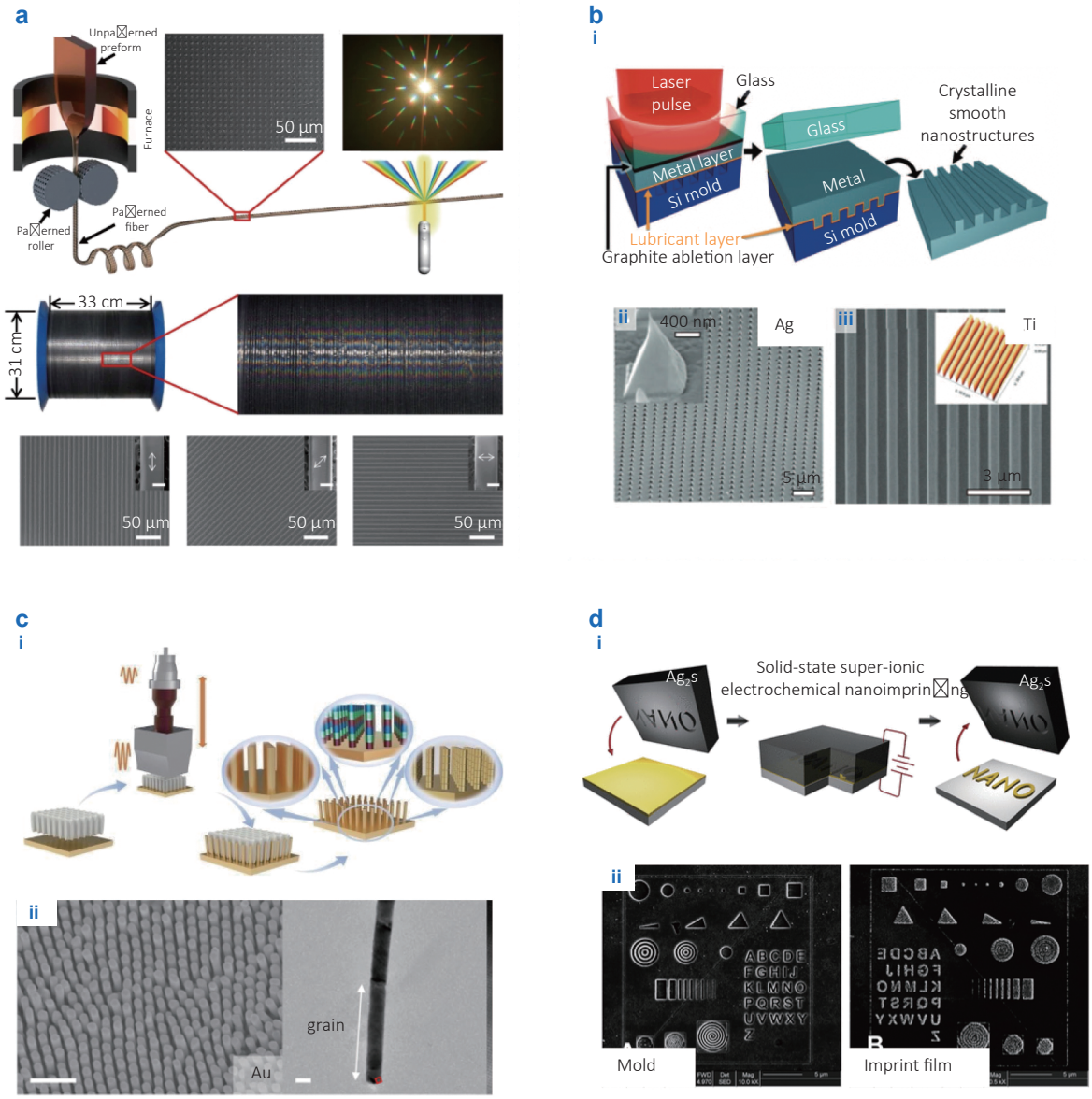

Fig. 11 | Different variations of NIL. (**a**) NIL for high throughput polymer fiber patterning. (**b**) Laser nanoimprinting. (**c**) Ultrasonic nanoimprinting. (**d**) Electrochemical imprinting. Figure reproduced with permission from: (a) ref.[182], (b) ref.[184], (c) ref. [185], under a Creative Commons licences; (d) ref.[186], American Chemical Society.

Chou et al. demonstrated the laser-assisted direct imprint (LADI) method to pattern Si with sub-10 nm resolution[183]. In this method, a single XeCl excimer laser pulse was used to melt a thin surface layer of silicon. Subsequently, a mold made of quartz was embossed into the low-viscosity molten Si liquid layer and was separated after Si was solidified. The low viscosity Si features render the intriguing characteristics of LADI—sub-10 nm resolution, sub-250 ns processing time, and excellent imprint of large, isolated patterns. Gao et al. utilized laser shock imprinting (LSI) to achieve high-resolution and smooth crystalline metal patterning, as shown in Fig. 11(b)[184]. In this method, a high-power ns-pulsed laser was used to irradiate an ablation coating layer, which sublimated and generated a shock wave with high pressure (0.85–1.83 GPa) to compress metal sheets into a nano-patterned silicon mold conformably. LSI doesn't suffer from the metal grain effect, and the patterning resolution can thus be high (< 30 nm). Figure 11(b-ii) shows the silver nanopyramid nanostructures fabricated by LSI. The sharp tips of the nanopyramids resulting from the high fabrication resolution of LSI are directly related to the device's performance on Surface-enhanced Raman scattering (SERS). LSI is also suitable for patterning hard metals, such as Ti, with a melting temperature of 1668 °C, as shown in Fig. 11(b-iii).

Ultrasound imprinting

Ultrasound imprinting is another method to pattern hard

material, like crystalline metal, at room temperature with nano-scaled resolution[185]. The working principle is demonstrated in Fig. 11(c-i). Like a jackhammer, the ultrasound imprinting method uses a high-frequency ultrasonic strike with the nanostructured mold to deform the materials, allowing the user to make nanostructures out of almost all solid materials regardless of their melting points, chemical reactivity, and ductility.

With ultrasound nanoimprinting, vertically aligned metal nanowires (Au, Ag, Sn, and Cu) with varying lengths (100 nm-10 μm) and diameters (30 nm-300 nm) can be obtained within 1 minute. The length of the nanowires can be tuned by adjusting the imprinting force and vibration amplitude. At the same time, the diameter is determined by the imprinting mold. Ultrasound nanoimprinting also allows for the fabrication of heterojunction nanowires composed of different materials with different properties, as shown in Fig. 11(c-ii). A nanowire array with Sn-Au junctions can be made regardless of a significant difference between the melting points. Metal and plastic heterojunction was also demonstrated. As a demonstration, the fabricated nanorods containing Ag-alumina-Ag heterojunctions were used as a SERS platform for quorum sensing.

Electrochemical nanoimprinting

Unlike the previously listed methods focusing on physically pressing and molding, electrochemical imprinting uses chemical reactions to achieve patterning. This method allows the direct patterning of rigid materials, such as semiconductor materials or metals. Figure 11(d-i)[186] illustrates the working principle of electrochemical imprinting. A patterned stamp made of a superionic conductor with a mobile cation is pressed into contact with the metallic substrate with pressure. After applying an electrical bias to the system, an electrochemical reaction is triggered and oxidizes the silver atoms on the substrate, progressively forming inverse features on the substrate. This method allows the pattern of 200 nm circles, as shown in Fig. 11(d-ii). Similar ideas can be used to pattern the semiconductor materials[187]. When pressing a patterned polymer mold coated with Pt thin film against an *n*-GaAs wafer with pressure, an intrinsic electric field is formed at the Pt/*n*-GaAs interface due to the difference in their work functions, triggering the redox-catalyzed dissolution of *n*-GaAs without any external energy modulation.

Conclusion

Nanoimprint lithography (NIL) has made tremendous progress over the past 30 years. Its advantages—high resolution, high throughput, complex 3D structuring, and one-step patterning—make it a unique technology suitable for various applications. NIL is currently under active evaluation by advanced semiconductor manufacturing foundries, capitalizing on its high resolution and low cost of ownership. The 3D capability also reduces the process steps required for manufacturing metal interconnect layers in semiconductor production. NIL is crucial in emerging optical applications like flat optics and augmented reality (AR) glasses. Its high-resolution capability enables the fabrication of high-efficiency metalenses, which have already been successfully commercialized. Furthermore, the 3D patterning feature makes NIL an ideal solution for the mass production of diffractive waveguides in AR glasses. NIL is also widely utilized in wafer-level optics, display technologies, optoelectronics, and biomedical applications. Notably, applications such as nanopatterning on curved surfaces benefit from NIL's flexible mold properties.

The long-standing defect issues in NIL have been significantly mitigated over the past three decades. Repeated defects, primarily caused by mold damage from foreign particles, which resulted in continuous imprinting defects at the same locations, have been addressed. Methods such as air filtration, soft mold imprinting, and using working stamps have been widely implemented to prevent these recurring defects. Random defects, typically arising from air trapping and non-conformal contact between the mold and substrate, have been minimized through strategies like high surface-energy resist, substrate conformal imprinting, and air cushions for pressing. Specialized companies in mold fabrication, resist development, imprinting tools, simulation toolboxes, defect detection, and application-related intellectual property have established a comprehensive NIL ecosystem.

In addition to its manufacturing advantages, NIL holds significant research value. It enables the patterning of various materials, including polymers, dielectric sol-gel solutions, composite metals, and crystalline metals, providing versatile functionalities. NIL also allows the modulation of polymer molecular chain alignment using different molds, enhancing device performance. The pressing process in NIL can be employed to engineer strain during nanopatterning, which aids in improving carrier mobility. Additionally, NIL is ideal for manufacturing high-*Q*-factor optical devices due to its high resolution and low lithography-induced edge roughness.

Looking ahead, many opportunities lie ahead for NIL. As the industry matures, the cost of ownership is expected to decrease further. The continued maturation of NIL will attract more attention and resources, further expanding the application of NIL.

References

1. Chou SY, Krauss PR, Renstrom PJ. Imprint of sub - 25 nm vias and trenches in polymers. *Appl Phys Lett* **67**, 3114–3116 (1995).
2. Chou SY, Krauss PR, Renstrom PJ. Imprint Lithography with 25-nanometer resolution. *Science* **272**, 85–87 (1996).
3. Chou SY, Krauss PR, Kong LS. Nanolithographically defined magnetic structures and quantum magnetic disk (invited). *J Appl Phys* **79**, 6101–6106 (1996).
4. Chou SY, Krauss PR, Zhang W et al. Sub-10 nm imprint lithography and applications. *J Vac Sci Technol B* **15**, 2897–2904 (1997).
5. Austin MD, Ge HX, Wu W et al. Fabrication of 5nm linewidth and

14nm pitch features by nanoimprint lithography. *Appl Phys Lett* **84**, 5299–5301 (2004).
6. Chou SY, Krauss PR. Imprint lithography with sub-10 nm feature size and high throughput. *Microelectron Eng* **35**, 237–240 (1997).
7. Chou SY, Krauss PR, Renstrom PJ. Nanoimprint lithography. *J Vac Sci Technol B* **14**, 4129–4133 (1996).
8. Li MT, Chen L, Chou SY. Direct three-dimensional patterning using nanoimprint lithography. *Appl Phys Lett* **78**, 3322–3324 (2001).
9. Sun XY, Zhuang L, Zhang W et al. Multilayer resist methods for nanoimprint lithography on nonflat surfaces. *J Vac Sci Technol B* **16**, 3922–3925 (1998).
10. Tan H, Gilbertson A, Chou SY et al. Roller nanoimprint lithography. *J Vac Sci Technol B* **16**, 3926–3928 (1998).
11. Chou SY. Patterned magnetic nanostructures and quantized magnetic disks. *Proc IEEE* **85**, 652–671 (1997).
12. Krauss PR, Chou SY. Nano-compact disks with 400 Gbit/in^2 storage density fabricated using nanoimprint lithography and read with proximal probe. *Appl Phys Lett* **71**, 3174–3176 (1997).
13. Guo LJ, Krauss PR, Chou SY. Nanoscale silicon field effect transistors fabricated using imprint lithography. *Appl Phys Lett* **71**, 1881–1883 (1997).
14. Wang J, Schablitsky S, Yu ZN et al. Fabrication of a new broadband waveguide polarizer with a double-layer 190 nm period metal-gratings using nanoimprint lithography. *J Vac Sci Technol B* **17**, 2957–2960 (1999).
15. Austin MD, Chou SY. Fabrication of 70 nm channel length polymer organic thin-film transistors using nanoimprint lithography. *Appl Phys Lett* **81**, 4431–4433 (2002).
16. Cao H, Yu ZN, Wang J et al. Fabrication of 10 nm enclosed nanofluidic channels. *Appl Phys Lett* **81**, 174–176 (2002).
17. Haisma J, Verheijen M, van den Heuvel K et al. Mold‐assisted nanolithography: a process for reliable pattern replication. *J Vac Sci Technol B* **14**, 4124–4128 (1996).
18. Colburn M, Johnson SC, Stewart MD et al. Step and flash imprint lithography: a new approach to high-resolution patterning. *Proc SPIE* **3676**, 379–389 (1999).
19. Ahn SH, Guo LJ. High-speed roll-to-roll nanoimprint lithography on flexible plastic substrates. *Adv Mater* **20**, 2044–2049 (2008).
20. Lebib A, Chen Y, Bourneix J et al. Nanoimprint lithography for a large area pattern replication. *Microelectron Eng* **46**, 319–322 (1999).
21. Heidari B, Maximov I, Montelius L. Nanoimprint lithography at the 6 in. wafer scale. *J Vac Sci Technol B* **18**, 3557–3560 (2000).
22. LaPedus M. Nano-imprint lithography added to ITRS roadmap – EE| Times. https://www.eetimes.com/nano-imprint-lithography-added-to-itrs-roadmap/.
23. McMackin I, Choi J, Schumaker P et al. Step and repeat UV nanoimprint lithography tools and processes. *Proc SPIE* **5374**, 222–231 (2004).
24. Verschuuren MA, Megens M, Ni YF et al. Large area nanoimprint by substrate conformal imprint lithography (SCIL). *Adv Opt Technol* **6**, 243–264 (2017).
25. Li ZW, Gu YN, Wang L et al. Hybrid nanoimprint-soft lithography with sub-15 nm resolution. *Nano Lett* **9**, 2306–2310 (2009).
26. Yang XM, Xu Y, Seiler C et al. Toward 1 Tdot/in.^{2} nanoimprint lithography for magnetic bit-patterned media: opportunities and challenges. *J Vac Sci Technol B* **26**, 2604–2610 (2008).
27. Ootera Y, Yuzawa A, Shimada T et al. Nanoimprint process for 2.5Tb/in^2 bit patterned media fabricated by self-assembling method. *Proc SPIE* **7970**, 79700K (2011).
28. Cheng X, Hong Y, Kanicki J et al. High-resolution organic polymer light-emitting pixels fabricated by imprinting technique. *J Vac Sci Technol B* **20**, 2877–2880 (2002).
29. Unno N, Mäkelä T. Thermal nanoimprint lithography—a review of the process, mold fabrication, and material. *Nanomaterials* **13**, 2031 (2023).
30. Chao CY, Fung W, Guo LJ. Polymer microring resonators for biochemical sensing applications. *IEEE J Sel Top Quantum Electron* **12**, 134–142 (2006).
31. Guo JP, Shaw MJ, Vawter GA et al. High-Q microring resonator for biochemical sensors. *Proc SPIE* **5728**, 83–92 (2005).
32. Chao CY, Guo LJ. Polymer microring resonators fabricated by nanoimprint technique. *J Vac Sci Technol B* **20**, 2862–2866 (2002).
33. Tu X, Chen SL, Song CL et al. Ultrahigh *Q* polymer microring resonators for biosensing applications. *IEEE Photonics J* **11**, 4200110 (2019).
34. Chen SL. Optical microring resonators for photoacoustic imaging and detection (University of Michigan, Ann Arbor, 2012).
35. Guo LJ. Recent progress in nanoimprint technology and its applications. *J Phys D Appl Phys* **37**, R123–R141 (2004).
36. Kwon B, Kim JH. Importance of molds for nanoimprint lithography: hard, soft, and hybrid molds. *J Nanosci* **2016**, 6571297 (2016).
37. Zhang C, Subbaraman H, Li QC et al. Printed photonic elements: nanoimprinting and beyond. *J Mater Chem C* **4**, 5133–5153 (2016).
38. Cheng X, Guo LJ. One-step lithography for various size patterns with a hybrid mask-mold. *Microelectron Eng* **71**, 288–293 (2004).
39. Guo LJ. Nanoimprint lithography: methods and material requirements. *Adv Mater* **19**, 495–513 (2007).
40. Pelloquin S, Augé S, Sharshavina K et al. Soft mold nanoImprint lithography: a versatile tool for sub-wavelength grating applications. In *Proceedings of 2017 Symposium on Design, Test, Integration and Packaging of MEMS/MOEMS* (IEEE, 2017). doi: 10.1109/DTIP.2017.7984454.
41. Bhingardive V, Menahem L, Schvartzman M. Soft thermal nanoimprint lithography using a nanocomposite mold. *Nano Res* **11**, 2705–2714 (2018).
42. Pandey A, Tzadka S, Yehuda D et al. Soft thermal nanoimprint with a 10 nm feature size. *Soft Matter* **15**, 2897–2904 (2019).
43. Barcelo S, Li ZY. Nanoimprint lithography for nanodevice fabrication. *Nano Converg* **3**, 21 (2016).
44. Sreenivasan SV. Nanoimprint lithography steppers for volume fabrication of leading-edge semiconductor integrated circuits. *Microsyst Nanoeng* **3**, 17075 (2017).
45. Zhang W, Fletcher B, Thompson E et al. High throughput Jet and Flash Imprint Lithography for semiconductor memory applications. *Proc SPIE* **9777**, 97770A (2016).
46. Wu W, Tong WM, Bartman J et al. Sub-10 nm nanoimprint lithography by wafer bowing. *Nano Lett* **8**, 3865–3869 (2008).
47. Gao H, Tan H, Zhang W et al. Air cushion press for excellent uniformity, high yield, and fast nanoimprint across a 100 mm field. *Nano Lett* **6**, 2438–2441 (2006).
48. Li H, Dong BQ, Zhang X et al. Disposable ultrasound-sensing chronic cranial window by soft nanoimprinting lithography. *Nat Commun* **10**, 4277 (2019).
49. Zhang Y, Feng WJ, Zhu WK et al. Universal color retrofit to polymer-based radiative cooling materials. *ACS Appl Mater Interfaces* **15**, 21008–21015 (2023).
50. Con C, Zhang J, Jahed Z et al. Thermal nanoimprint lithography using fluoropolymer mold. *Microelectron Eng* **98**, 246–249 (2012).
51. Williams SS, Retterer S, Lopez R et al. High-resolution PFPE-based molding techniques for nanofabrication of high-pattern density, Sub-20 nm features: a fundamental materials approach. *Nano Lett* **10**, 1421–1428 (2010).

52. Kooy N, Mohamed K, Pin LT et al. A review of roll-to-roll nanoimprint lithography. *Nanoscale Res Lett* **9**, 320 (2014).
53. Haslinger MJ, Moharana AR, Mühlberger M. Antireflective moth-eye structures on curved surfaces fabricated by nanoimprint lithography. *Proc SPIE* **11177**, 111770K (2019).
54. Lin WK, Liu S, Lee S et al. High *Q*-factor polymer microring resonators realized by versatile damascene soft nanoimprinting lithography. *Adv Funct Mater* **34**, 2312229 (2024).
55. Pina-Hernandez C, Kim JS, Guo LJ et al. High-throughput and etch-selective nanoimprinting and stamping based on fast-thermal-curing poly(dimethylsiloxane)s. *Adv Mater* **19**, 1222–1227 (2007).
56. Thanner C, Eibelhuber M. UV nanoimprint lithography: geometrical impact on filling properties of nanoscale patterns. *Nanomaterials* **11**, 822 (2021).
57. Selinidis KS, Brooks CB, Doyle GF et al. Mask replication using jet and flash imprint lithography. *J Micro/Nanolithogr MEMS MOEMS* **10**, 043005 (2011).
58. Einck VJ, Torfeh M, McClung A et al. Scalable nanoimprint lithography process for manufacturing visible metasurfaces composed of high aspect ratio TiO_2 meta-atoms. *ACS Photonics* **8**, 2400–2409 (2021).
59. Choi H, Kim J, Kim W et al. Realization of high aspect ratio metalenses by facile nanoimprint lithography using water-soluble stamps. *PhotoniX* **4**, 18 (2023).
60. Obducat. SINDRE® Integra. https://www.obducat.com/products-foundry-services/sindre-2/.
61. EVG. EVG®770 NT. https://www.evgroup.com/products/nanoimprint-lithography/uv-nil-smartnil/evg770-nt.
62. Pina-Hernandez C, Fu PF, Guo LJ. Ultrasmall structure fabrication *via* a facile size modification of nanoimprinted functional silsesquioxane features. *ACS Nano* **5**, 923–931 (2011).
63. Miebori T, Unno N, Taniguchi J. Super resolution technique for sub-100 nm nanoimprint mold via mechanical deformation method. *Microelectron Eng* **123**, 38–42 (2014).
64. Lee SH, Jang B, Guo LJ. Large-scale mold preparation for R2R systems by a novel mold replication and global shrinking process. In *Proceedings of the 2021 International Conference on Micro- and Nano-Devices Enabled by R2R Manufacturing* (2021).
65. Pina-Hernandez C, Guo LJ, Fu PF. High-resolution functional epoxysilsesquioxane-based patterning layers for large-area nanoimprinting. *ACS Nano* **4**, 4776–4784 (2010).
66. Dundar Arisoy F, Czolkos I, Johansson A et al. Low-cost, durable master molds for thermal-NIL, UV-NIL, and injection molding. *Nanotechnology* **31**, 015302 (2020).
67. Ma PS, Xu Z, Wang M et al. Fast fabrication of TiO_2 hard stamps for nanoimprint lithography. *Mater Res Bull* **90**, 253–259 (2017).
68. Zhang GM, Zhang J, Xie GY et al. Cicada wings: a stamp from nature for nanoimprint lithography. *Small* **2**, 1440–1443 (2006).
69. Nowduri B, Schulte S, Decker D et al. Biomimetic nanostructures fabricated by nanoimprint lithography for improved cell-coupling. *Adv Funct Mater* **30**, 2004227 (2020).
70. Yoon G, Kim K, Huh D et al. Single-step manufacturing of hierarchical dielectric metalens in the visible. *Nat Commun* **11**, 2268 (2020).
71. Zhang JZ, Hu X, Zhang J et al. A fast thermal-curing nanoimprint resist based on cationic polymerizable epoxysiloxane. *Nanoscale Res Lett* **7**, 380 (2012).
72. Schuster C, Reuther F, Kolander A et al. mr-NIL 6000LT–Epoxy-based curing resist for combined thermal and UV nanoimprint lithography below 50 °C. *Microelectron Eng* **86**, 722–725 (2009).
73. Yu CC, Chen HL. Nanoimprint technology for patterning functional materials and its applications. *Microelectron Eng* **132**, 98–119 (2015).
74. Ready-to-use Formulations for Thermal & Photo (UV) Nanoimprint Lithography (NIL).
75. Cox LM, Martinez AM, Blevins AK et al. Nanoimprint lithography: emergent materials and methods of actuation. *Nano Today* **31**, 100838 (2020).
76. Das Gupta T, Martin-Monier L, Yan W et al. Self-assembly of nanostructured glass metasurfaces via templated fluid instabilities. *Nat Nanotechnol* **14**, 320–327 (2019).
77. Lin XH, Ling T, Subbaraman H et al. Ultraviolet imprinting and aligned ink-jet printing for multilayer patterning of electro-optic polymer modulators. *Opt Lett* **38**, 1597–1599 (2013).
78. Wang Y, Tsiminis G, Kanibolotsky AL et al. Nanoimprinted polymer lasers with threshold below 100 W/cm^2 using mixed-order distributed feedback resonators. *Opt Express* **21**, 14362–14367 (2013).
79. Hu ZJ, Tian MW, Nysten B et al. Regular arrays of highly ordered ferroelectric polymer nanostructures for non-volatile low-voltage memories. *Nat Mater* **8**, 62–67 (2009).
80. Kothari R, Beaulieu MR, Hendricks NR et al. Direct patterning of robust one-dimensional, two-dimensional, and three-dimensional crystalline metal oxide nanostructures using imprint lithography and nanoparticle dispersion inks. *Chem Mater* **29**, 3908–3918 (2017).
81. Kim J, Kim W, Oh DK et al. One-step printable platform for high-efficiency metasurfaces down to the deep-ultraviolet region. *Light Sci Appl* **12**, 68 (2023).
82. Kim J, Kim W, Choi M et al. Amorphous to crystalline transition in nanoimprinted sol–gel titanium oxide metasurfaces. *Adv Mater* **36**, 2405378 (2024).
83. Modaresialam M, Chehadi Z, Bottein T et al. Nanoimprint lithography processing of inorganic-based materials. *Chem Mater* **33**, 5464–5482 (2021).
84. Rimböck J, Schuster P, Vsetecka L et al. UV nanoimprint lithography—impact of coating techniques on pattern quality. *Nanomanufacturing* **4**, 69–80 (2024).
85. Williams BR, Pierce J, Black K et al. Process repeatability in volume manufacturing of nanostructures utilizing nanoimprint lithography. *Proc SPIE* **11467**, 114670D (2020).
86. Achleitner T, Rimböck J, Vsetecka L et al. Inkjet coating combined with nanoimprinting for complex 3D patterns with progressive height increase and low residual layer. *Proc SPIE* **12956**, 1295608 (2024).
87. Ifuku T, Yonekawa M, Nakagawa K et al. Nanoimprint lithography performance advances for new application spaces. *Proc SPIE* **12956**, 1295603 (2024).
88. Ballottin M, Jansen N, Scheidegger A et al. Practical considerations for large-area nanoimprinted augmented reality waveguides. *Proc SPIE* **12957**, 129570J (2024).
89. EVG. EVG®7200 LA. https://www.evgroup.com/products/nanoimprint-lithography/uv-nil-smartnil/evg-7200-la.
90. Lan HB. Large-area nanoimprint lithography and applications. In Thirumalai J. *Micro/Nanolithography - A Heuristic Aspect on the Enduring Technology* (IntechOpen, 2017). doi: 10.5772/INTECHOPEN.72860.
91. Obducat. Obducat´s product portfolio. https://www.obducat.com/products-foundry-services/product-portfolio/.
92. Thanner C, Dudus A, Treiblmayr D et al. Nanoimprint lithography for augmented reality waveguide manufacturing. *Proc SPIE* **11310**, 1131010 (2020).

93. Ahn SH, Guo LJ. Large-area roll-to-roll and roll-to-plate Nanoimprint Lithography: a step toward high-throughput application of continuous nanoimprinting. *ACS Nano* **3**, 2304–2310 (2009).
94. Thanner C, Bichler A, Feichtlbauer F et al. Step and repeat imprint lithography for wafer scale mastering of micro-and nanostructures. In *Proceedings of 2022 International Semiconductor Conference* 69–72 (IEEE, 2022).
95. Ye ZM, Luo K, Irving JW et al. Defect reduction for semiconductor memory applications using jet and flash imprint lithography. *Proc SPIE* **8680**, 86800C (2013).
96. Yamamoto K, Wada H, Suzaki Y et al. Nanoimprint lithography methods for achieving sub-3 nm overlay. *Proc SPIE* **11855**, 1185509 (2021).
97. Chen IT, Schappell E, Zhang XL et al. Continuous roll-to-roll patterning of three-dimensional periodic nanostructures. *Microsyst Nanoeng* **6**, 22 (2020).
98. Ahn SH, Miller M, Yang SQ et al. High volume nanoscale roll-based imprinting using jet and flash imprint lithography. *Proc SPIE* **9049**, 90490G (2014).
99. Ogusu M, Ishida M, Tamura M et al. Nanoimprint edge placement error elements and control. *Proc SPIE* **12054**, 1205405 (2022).
100. Schuster P, Rimböck J, Vsetecka L et al. Inkjet coating combined with nanoimprinting for complex 3D patterns with nonlinear height and low residual layer. *Proc SPIE* **13414**, 134140E (2025).
101. Park Y, Kim J, Yang Y et al. Tape-assisted residual layer-free one-step nanoimprinting of high-index hybrid polymer for optical loss-suppressed metasurfaces. *Adv Sci* **12**, 2409371 (2025).
102. Pina-Hernandez C, Kim JS, Fu PF et al. Nonresidual layer imprinting and new replication capabilities demonstrated for fast thermal curable polydimethysiloxanes. *J Vac Sci Technol B* **25**, 2402–2406 (2007).
103. Nakayama T, Yonekawa M, Matsuoka Y et al. Improved defectivity and particle control for nanoimprint lithography high-volume semiconductor manufacturing. *Proc SPIE* **10144**, 1014407 (2017).
104. Ito T, Zhang W, Liu WJ. Reduction of non-fill defects in nanoimprint lithography. *Jpn J Appl Phys* **63**, 050804 (2024).
105. Takabayashi Y, Iwanaga T, Hiura M et al. Nanoimprint system alignment and overlay improvement for high volume semiconductor manufacturing. *Proc SPIE* **10958**, 109580B (2019).
106. Jin H, Qi YJ. Review of overlay error and controlling methods in alignment system for advanced lithography. *Proc SPIE* **12478**, 1247843 (2022).
107. Torii H, Hiura M, Takabayashi Y et al. Nanoimprint lithography: today and tomorrow. *Proc SPIE* **12054**, 1205403 (2022).
108. Canon Global. FPA-1200NZ2C. https://global.canon/en/product/indtech/semicon/fpa1200nz2c.html.
109. Maruyama N, Sato K, Suzaki Y et al. Advances and applications in nanoimprint lithography. *Proc SPIE* **12497**, 124970D (2023).
110. Takeuchi N, Hasegawa G, Komukai T et al. Fabrication of dual damascene structure with nanoimprint lithography and dry-etching. *Proc SPIE* **12497**, 124970E (2023).
111. Traub MC, Longsine W, Truskett VN. Advances in nanoimprint lithography. *Annu Rev Chem Biomol Eng* **7**, 583–604 (2016).
112. Tanaka H, Maruyama N, Hiura M et al. Establishing a nanoimprint lithography ecosystem. *Proc SPIE* **12751**, 127510D (2023).
113. Ifuku T, Hiura M, Takabayashi Y et al. Nanoimprint performance improvements for high volume semiconductor device manufacturing. *Proc SPIE* **12293**, 122930E (2022).
114. Kono T, Hatano M, Tokue H et al. Half-pitch 14 nm direct patterning with nanoimprint lithography. *Proc SPIE* **10958**, 109580H (2019).
115. Kobayashi S, Yamashita K, Tsuda H et al. Design for nanoimprint lithography: hot spot modification through total NIL process simulation. *Proc SPIE* **10584**, 105840R (2018).
116. Techovedas. Micron supports canon nano-semiconductor printing for DRAM; threatening ASML monopoly. https://techovedas.com/micron-supports-canon-nano-semiconductor-printing-for-dram-threatening-asml-monopoly/.
117. Mitsuyasu M, Takeuchi N, Hirose M et al. Preliminary qualification of 3D nanoimprint process for dual damascene wiring. *Proc SPIE* **PC12956**, PC129560G (2024). doi: 10.1117/12.3010093.
118. Chou SY. Nanoimprint technology for patterned magnetic nanostructures: novel techniques for characterizing and preparing samples nanomagnetism —application and characterization. In Kronmüller H, Parkin S. *Handbook of Magnetism and Advanced Magnetic Materials* (Wiley, Hoboken, 2007). doi: 10.1002/9780470022184.HMM324.
119. Marigo L, Quaade U, Schmidlin M. Flat optics for compact integration and high performances. *Proc SPIE* **12402**, 1240209 (2023).
120. Patoux A, Agez G, Girard C et al. Challenges in nanofabrication for efficient optical metasurfaces. *Sci Rep* **11**, 5620 (2021).
121. Mattinson F, Quaade U, Johansen VE et al. Latest advancements at NILT on flat metalens based camera modules in near infrared. *Proc SPIE* **12217**, 1221707 (2022).
122. Williams BR, Bacon-Brown D, George M et al. Progress in commercializing visible wavelength metalenses. *Proc SPIE* **PC13109**, PC1310911 (2024). doi: 10.1117/12.3028131.
123. Williams BR, Bacon-Brown D, George MCC et al. NIL enabled mass production of visible meta-optics. *Proc SPIE* **PC12898**, PC128980U (2024). doi: 10.1117/12.3008763.
124. Kim J, Seong J, Kim W et al. Scalable manufacturing of high-index atomic layer–polymer hybrid metasurfaces for metaphotonics in the visible. *Nat Mater* **22**, 474–481 (2023).
125. Quaade U, Egede Johansen V, Llinas JM et al. Highly efficient metalenses for imaging applications at infrared wavelengths. *Proc SPIE* **PC12010**, PC1201012 (2022). doi: 10.1117/12.2624414.
126. Bilenberg B. Meta optical elements produced by nanoimprint lithography. *Proc SPIE* **PC12054**, PC120540W (2022). doi: 10.1117/12.2617835.
127. Yang WH, Zhou JX, Tsai DP et al. Advanced manufacturing of dielectric meta-devices. *Photonics Insights* **3**, R04 (2024).
128. Yoon G, Kim K, Kim SU et al. Printable nanocomposite metalens for high-contrast near-infrared imaging. *ACS Nano* **15**, 698–706 (2021).
129. Gong JT, Xiong LX, Pu MB et al. Visible meta-displays for anti-counterfeiting with printable dielectric metasurfaces. *Adv Sci* **11**, 2308687 (2024).
130. Gong JT, Xiong LX, Zhang F et al. Integrated quad-color nanoprinting and tri-channel holographic encryption meta-marks with printable metasurfaces. *Laser Photonics Rev* **19**, 2401045 (2025).
131. Gong JT, Xiong XL, Pu MB et al. High-throughput fabrication of curved plasmonic metasurfaces for switchable beam focusing and thermal infrared cloaking. *Adv Opt Mater* **11**, 2300608 (2023).
132. Jung DE, Howell IR, Einck VJ et al. Refractive index tuning of all-inorganic TiO_2 nanocrystal-based films and high aspect ratio nanostructures using atomic layer deposition: implications for high-throughput fabrication of metalenses. *ACS Appl Nano Mater* **6**, 2009–2019 (2023).
133. Eon Jung D, Einck VJ, Dawicki A et al. Full wafer scale manufacturing of directly printed TiO_2 metalenses at visible wavelengths with outstanding focusing efficiencies. *Adv Mater* 2500327 (2025) doi: 10.1002/ADMA.202500327.
134. Carden S. High performance at scale: unlocking waveguide production for AR. *Proc SPIE* **12450**, 1245012 (2023).

135. Ding YQ, Yang Q, Li YNQ et al. Waveguide-based augmented reality displays: perspectives and challenges. *eLight* **3**, 24 (2023).
136. Achleitner T, Rimböck J, Vsetecka L et al. Inkjet coating combined with nanoimprinting for complex 3D patterns with progressive height increase and low residual layer. *Proc SPIE* **12956**, 1295608 (2024). doi: 10.1117/12.3009889.
137. Steiner S, Jotz M, Bachhuber F et al. Enabling mass manufacturing of industry-standard optical waveguide combiners. *J Opt Microsyst* **3**, 033502 (2023).
138. Kress BC. Optical waveguide combiners for AR headsets: features and limitations. *Proc SPIE* **11062**, 110620J (2019).
139. Photonics Spectra. Full-immersion AR: the path to consumer-friendly devices. https://www.photonics.com/Articles/Full-Immersion_AR_The_Path_to_Consumer-Friendly/a65320.
140. Tadros NJ, Krieg A, Cade J et al. PixNIL high index nanocomposite materials with improved processability for large volume manufacturing. *Proc SPIE* **12913**, 1291305 (2024).
141. McCoy JA, Verschuuren MA, Miles DM et al. X-ray verification of sol-gel resist shrinkage in substrate-conformal imprint lithography for a replicated blazed reflection grating. *OSA Continuum* **3**, 3141–3156 (2020).
142. Souri M, Ip V, Falmbigl M et al. Reactive ion beam etch of highly uniform slanted gratings for augmented reality applications. *Proc SPIE* **PC12913**, PC129130M (2024). doi: 10.1117/12.3001026.
143. Pina-Hernandez C, Yamada K, Legacy A et al. Ultra-high refractive index materials for patterning diffractive optical elements with nanoimprint lithography. *Proc SPIE* **12449**, 1244905 (2023).
144. Lan S. Wafer level nano-optics solution for AR glasses. *Proc SPIE* **12914**, 1291416 (2024).
145. EVG. Wafer-level micro-optics fabrication by lens molding using UV-curable polymers. https://www.evgroup.com/fileadmin/media/downloads/2023/White_Paper-EVG-DELO_Wafer-level_micro-optics-fabrication.pdf.
146. Dannberg P, Wippermann F, Brückner A et al. Wafer-level hybrid integration of complex micro-optical modules. *Micromachines* **5**, 325–340 (2014).
147. Photonics Spectra. High-precision wafer-level optics fabrication and integration. https://www.photonics.com/Articles/High-Precision_Wafer-Level_Optics_Fabrication_and/a45233.
148. Brehm M, Ertl C, Pilottek I et al. UV curing materials for wafer level optics. *Proc SPIE* **11292**, 112920I (2020).
149. Nakamura T, Yang Z, Ogawa D et al. “Better than DOE optics” solution in ToF sensors for wearable XR device. *Proc SPIE* **12449**, 1244911 (2023).
150. Israel A, Ulfan F, Pascar L et al. Photonic plug for scalable silicon photonics packaging. *Proc SPIE* **11286**, 1128607 (2020).
151. PIC Magazine News. Wafer-level nanoimprint technology for innovative packaging. https://picmagazine.net/article/115752/Wafer-level_nanoimprint_technology_for_innovative_packaging_.
152. Mitsubishi Chemical Group. Moth eye-type antireflective film MOSMITE™. https://www.m-chemical.co.jp/en/products/departments/mcc/industrial-medical/product/1201267_8054.html.
153. SCIVAX. White paper : wire grid polarizers using nanoimprint lithography. https://www.scivax.com/wp-content/uploads/2022/05/WGP_White-Paper_English.pdf.
154. Schleunitz A, Schift H. Fabrication of 3D nanoimprint stamps with continuous reliefs using dose-modulated electron beam lithography and thermal reflow. *J Micromech Microeng* **20**, 095002 (2010).
155. Schift H. Nanoimprint lithography: 2D or not 2D? A review. *Appl Phys A* **121**, 415–435 (2015).
156. SCIVAX. DFB laser diode. https://www.scivax.com/en/application/dfb/.
157. Mitsubishi Chemical Group. Allowing over 99% of light to pass through, making it virtually invisible. MOSMITE™ is a new material used for art and automotive displays. https://www.mcgc.com/english/kaiteki_solution_center/oursolution/15.html.
158. Ahn SH, Yang SQ, Miller M et al. High-performance wire-grid polarizers using jet and Flash™ imprint lithography. *J Micro/Nanolithogr MEMS MOEMS* **12**, 031104 (2013).
159. See the Possibilities™. Pixelated wire-grid polarizers. https://moxtek.com/optics-product/pixelated-polarizers/.
160. Hruska J. Amazon sheds new light on Kindle Paperwhite display. https://www.extremetech.com/electronics/137158-amazon-sheds-new-light-on-kindle-paperwhite-display.
161. Lee YC, Ni CH, Chen CY. Enhancing light extraction mechanisms of GaN-based light-emitting diodes through the integration of imprinting microstructures, patterned sapphire substrates, and surface roughness. *Opt Express* **18**, A489–A498 (2010).
162. Overton G. IQE nanoimprint lithography technology tapped for DFB laser production. https://www.laserfocusworld.com/lasers-sources/article/16571676/iqe-nanoimprint-lithography-technology-tapped-for-dfb-laser-production.
163. Xiong YF, Xu F. Multifunctional integration on optical fiber tips: challenges and opportunities. *Adv Photonics* **2**, 064001 (2020).
164. Kostovski G, Stoddart PR, Mitchell A. The optical fiber tip: an inherently light-coupled microscopic platform for micro- and nanotechnologies. *Adv Mater* **26**, 3798–3820 (2014).
165. Calafiore G, Koshelev A, Darlington TP et al. Campanile near-field probes fabricated by nanoimprint lithography on the facet of an optical fiber. *Sci Rep* **7**, 1651 (2017).
166. Koshelev A, Calafiore G, Piña-Hernandez C et al. High refractive index Fresnel lens on a fiber fabricated by nanoimprint lithography for immersion applications. *Opt Lett* **41**, 3423–3426 (2016).
167. HighRI Optics, Inc. Wavefront manipulation. https://highrioptics.com/applications-and-industries/wavefront-manipulation/.
168. HighRI Optics, Inc. Super-resolution imaging. https://highrioptics.com/applications-and-industries/super-resolution-imaging/.
169. Choi J, Lee CC, Park S. Scalable fabrication of sub-10 nm polymer nanopores for DNA analysis. *Microsyst Nanoeng* **5**, 12 (2019).
170. Fu XX, Cai JX, Zhang X et al. Top-down fabrication of shape-controlled, monodisperse nanoparticles for biomedical applications. *Adv Drug Deliv Rev* **132**, 169–187 (2018).
171. Chen JH, Zhou YL, Wang DH et al. UV-nanoimprint lithography as a tool to develop flexible microfluidic devices for electrochemical detection. *Lab Chip* **15**, 3086–3094 (2015).
172. Tegenfeldt JO, Prinz C, Cao H et al. Micro- and nanofluidics for DNA analysis. *Anal Bioanal Chem* **378**, 1678–1692 (2004).
173. Guo LJ, Cheng X, Chou CF. Fabrication of size-controllable nanofluidic channels by nanoimprinting and its application for DNA stretching. *Nano Lett* **4**, 69–73 (2004).
174. Zandi Shafagh R, Shen JX, Youhanna S et al. Facile nanoimprinting of robust high-aspect-ratio nanostructures for human cell biomechanics. *ACS Appl Bio Mater* **3**, 8757–8767 (2020).
175. Cheng LJ, Kao MT, Meyhöfer E et al. Highly efficient guiding of microtubule transport with imprinted CYTOP nanotracks. *Small* **1**, 409–414 (2005).

176. Hoff JD, Cheng LJ, Meyhöfer E et al. Nanoscale protein patterning by imprint lithography. *Nano Lett* **4**, 853–857 (2004).
177. Liu S, Lin WK, Zhang Y et al. Wafer-scale fabrication of ultra-low loss Si_3N_4 photonic integrated chips through nanoimprint lithography. *Adv Funct Mater* **7**, 622–626 (2013).
178. Bar-On O, Brenner P, Siegle T et al. High quality 3D photonics using nano imprint lithography of fast sol-gel materials. *Sci Rep* **8**, 7833 (2018).
179. Aryal M, Trivedi K, Hu WC. Nano-confinement induced chain alignment in ordered P3HT nanostructures defined by nanoimprint lithography. *ACS Nano* **3**, 3085–3090 (2009).
180. Sun CY, Zhong JW, Gan ZF et al. Nanoimprint-induced strain engineering of two-dimensional materials. *Microsyst Nanoeng* **10**, 49 (2024).
181. Wang YX, Jin SY, Wang QX et al. Parallel nanoimprint forming of one-dimensional chiral semiconductor for strain-engineered optical properties. *Nano-Micro Lett* **12**, 160 (2020).
182. Wang Z, Wu TT, Wang ZX et al. Designer patterned functional fibers via direct imprinting in thermal drawing. *Nat Commun* **11**, 3842 (2020).
183. Chou SY, Keimel C, Gu J. Ultrafast and direct imprint of nanostructures in silicon. *Nature* **417**, 835–837 (2002).
184. Gao H, Hu YW, Xuan Y et al. Large-scale nanoshaping of ultrasmooth 3D crystalline metallic structures. *Science* **346**, 1352–1356 (2014).
185. Ge JY, Ding B, Hou S et al. Rapid fabrication of complex nanostructures using room-temperature ultrasonic nanoimprinting. *Nat Commun* **12**, 3146 (2021).
186. Hsu KH, Schultz PL, Ferreira PM et al. Electrochemical nanoimprinting with solid-state superionic stamps. *Nano Lett* **7**, 446–451 (2007).
187. Zhang J, Zhang L, Han LH et al. Electrochemical nanoimprint lithography: when nanoimprint lithography meets metal assisted chemical etching. *Nanoscale* **9**, 7476–7482 (2017).

Acknowledgements

The authors would like to thank the National Science Foundation for the partial support (NSF-2213684), and LJG acknowledges an Emmett Leith Collegiate Professorship for this writing.

Competing interests

L. Jay Guo serves as an Editor for the Journal, and no other author has reported any competing interests.